The Fast Stochastic Matching Pursuit for Neutrino and Dark Matter Experiments

Yuyi Wang[1,2,3], Aiqiang Zhang[1,2,3], Yiyang Wu[1,2,3], Benda Xu[1,2,3*], Jiajie Chen[4], Zhe Wang[1,2,3], Shaomin Chen[1,2,3]

[1] Department of Engineering Physics, Tsinghua University, Beijing,100084,China.

[2] Center for High Energy Physics, Tsinghua University, Beijing,100084,China.

[3] Key Laboratory of Particle & Radiation Imaging (Tsinghua University), Ministry of Education, China.

[4] Department of Computer Science and Technology, Tsinghua University, Beijing,100084,China.

*Corresponding author(s). E-mail(s): orv@tsinghua.edu.cn;

Abstract

Photomultiplier tubes (PMT) are widely deployed at neutrino and dark matter experiments for photon counting. When multiple photons hit a PMT consecutively, their photo-electron (PE) pulses pile up to hinder the precise measurements of the count and timings. We introduce Fast Stochastic Matching Pursuit (FSMP) to analyze the PMT signal waveforms into individual PEs with the strategy of reversible-jump Markov-chain Monte Carlo. We demonstrate that FSMP improves the energy and time resolution of PMT-based experiments, gains acceleration on GPUs and is extensible to microchannel-plate (MCP) PMTs with jumbo-charge outputs. In the condition of our laboratory characterization of 8-inch MCP-PMTs, FSMP improves the energy resolution by up to 12 % from the long-serving method of waveform integration.

Keywords: waveform analysis, MCP-PMT, energy resolution, time resolution, GPU acceleration

A mid-infrared dual-comb spectrometer in step-sweep mode for high-resolution molecular spectroscopy

Muriel Lepère*[a], Olivier Browet[a], Jean Clément[a], Bastien Vispoel[a], Pitt Allmendinger[b], Jakob Hayden[b], Florian Eigenmann[b], Andreas Hugi[b], and Markus Mangold[b],
[a]Research unit Lasers and Spectroscopies (LLS), Institute of Life, Earth and Environment (ILEE), University of Namur, 61, Rue de Bruxelles, Namur, Belgium;
[b]IRsweep AG, Laubisrütistrasse 44, 8712 Stäfa, Switzerland

*muriel.lepere@unamur.be; phone +3281724496; https://www.unamur.be/en/sci/physics/ur-en/lls/

ABSTRACT

To meet the challenges of high-resolution molecular spectroscopy, increasingly sophisticated spectroscopic techniques were developed. For a long time FTIR and laser-based spectroscopies were used for these studies. The recent development of dual-comb spectroscopy at high-resolution makes this technique a powerful tool for gas phase studies. We report on the use and characterization of the IRis-F1, a tabletop mid-infrared dual-comb spectrometer, in the newly developed *step-sweep* mode. The resolution of the wavenumber axis is increased by step-wise tuning (interleaving) and accurate measurement of the laser center wavelength and repetition frequency. Doppler limited measurements of N_2O and CH_4 reveal a wavenumber accuracy of 10^{-4} cm^{-1} on the covered range of > 50 cm^{-1}. Measured half-widths of absorption lines show no systematic broadening, indicating a negligible instrument response function. Finally, measurements of nitrogen pressure broadening coefficients in the ν_4 band of methane show that quantum cascade laser dual-comb spectroscopy in *step-sweep* mode is well adapted for measurements of precision spectroscopic data, in particular line shape parameters.

1. INTRODUCTION

High-resolution molecular spectroscopy has both fundamental and applied interests. It allows understanding intra- and inter-molecular interactions in gas phase, and is a powerful tool to study planetary atmospheres. On Earth, atmospheric pollution and global warming are challenges for all societies around the world [1, 2]. Different instruments installed on various platforms (space satellites, stratospheric balloons, ground-based stations) are continuously monitoring the atmosphere to characterize it and unravel the mechanisms occurring. The retrieval of atmospheric spectra relies on the computation of the radiative transfer that in turn requires many chemical and physical parameters, among them the spectroscopic parameters and their temperature evolution. The recent improvements of remote sensing mission instruments have pushed the need for high accuracy spectroscopic data [3, 4], as the quality of the retrieved information depends on the precision of the spectroscopic parameters [5] for which the line-shape parameters are the largest sources of uncertainties [6-8].

High-resolution infrared spectrometers, such as high-resolution dual-comb spectrometers, are able to provide precise spectroscopic parameters. This data is also very important for the development and improvement of theoretical models describing molecular interactions. For decades, theoretical models have been developed and used [9] to describe the molecular interactions and to compute line-shape parameters. The models rely on intermolecular potentials that must be validated by accurate measurements. Theoretical models and laboratory measurements complement, challenge and boost each other in this quest to understand chemical and physical phenomena that occur in the gas phase. In particular, the mid-infrared spectral region is very interesting since the fundamental vibrational bands of many molecules are located in this spectral domain. At room temperature, these bands are the most intense; this allows a great precision in the measurements of spectroscopic data.

To meet the challenges of molecular spectroscopy, increasingly sophisticated spectroscopic techniques have been developed. They compete in a variety of often conflicting parameters such as good spectral resolution and large coverage, accurate absolute frequency calibration, and high signal-to-noise ratio at short measurement times. For a long time, Fourier transform spectroscopy (Ref. [10] and therein) was the workhorse for mid-infrared studies providing a lot of accurate line

Article

Performance of a modular ton-scale pixel-readout liquid argon time projection chamber

A. Abed Abud[1], B. Abi[2], R. Acciarri[3], M. A. Acero[4], M. R. Adames[5], G. Adamov[6], M. Adamowski[3], D. Adams[7], M. Adinolfi[8], C. Adriano[9], A. Aduszkiewicz[10], J. Aguilar[11], B. Aimard[12], F. Akbar[13], K. Allison[14], S. Alonso Monsalve[1,15], M. Alrashed[16], A. Alton[17], R. Alvarez[18], T. Alves[19], H. Amar[20], P. Amedo[21,20], J. Anderson[22], D. A. Andrade[23], C. Andreopoulos[24], M. Andreotti[25,26], M. P. Andrews[3], F. Andrianala[27], S. Andringa[28], N. Anfimov[29], A. Ankowski[30], M. Antoniassi[5], M. Antonova[20], A. Antoshkin[29], A. Aranda-Fernandez[31], L. Arellano[32], E. Arrieta Diaz[33], M. A. Arroyave[3], J. Asaadi[34], A. Ashkenazi[35], D. Asner[7], L. Asquith[36], E. Atkin[19], D. Auguste[37], A. Aurisano[38], V. Aushev[39], D. Autiero[40], F. Azfar[2], A. Back[41], H. Back[42], J. J. Back[43], I. Bagaturia[6], L. Bagby[3], N. Balashov[29], S. Balasubramanian[3], P. Baldi[44], W. Baldini[25], J. Baldonedo[45], B. Baller[3], B. Bambah[46], R. Banerjee[47], F. Barao[28,48], G. Barenboim[20], P. Barham Alzás[1], G. J. Barker[43], W. Barkhouse[49], G. Barr[2], J. Barranco Monarca[50], A. Barros[5], N. Barros[28,51], D. Barrow[2], J. L. Barrow[52], A. Basharina-Freshville[53], A. Bashyal[22], V. Basque[3], C. Batchelor[54], L. Bathe-Peters[2], J.B.R. Battat[55], F. Battisti[2], F. Bay[56], M. C. Q. Bazetto[9], J. L. L. Bazo Alba[57], J. F. Beacom[58], E. Bechetoille[40], B. Behera[59], E. Belchior[60], G. Bell[61], L. Bellantoni[3], G. Bellettini[62,63], V. Bellini[64,65], O. Beltramello[1], N. Benekos[1], C. Benitez Montiel[20,66], D. Benjamin[7], F. Bento Neves[28], J. Berger[67], S. Berkman[68], J. Bernal[66], P. Bernardini[69,70], A. Bersani[71], S. Bertolucci[72,73], M. Betancourt[3], A. Betancur Rodríguez[74], A. Bevan[75], Y. Bezawada[76], A. T. Bezerra[77], T. J. Bezerra[36], A. Bhat[78], V. Bhatnagar[79], J. Bhatt[53], M. Bhattacharjee[80], M. Bhattacharya[3], S. Bhuller[8], B. Bhuyan[80], S. Biagi[81], J. Bian[44], K. Biery[3], B. Bilki[82,83], M. Bishai[7], A. Bitadze[32], A. Blake[84], F. D. Blaszczyk[3], G. C. Blazey[85], E. Blucher[78], J. Bogenschuetz[34], J. Boissevain[86], S. Bolognesi[87], T. Bolton[16], L. Bomben[88,89], M. Bonesini[88,90], C. Bonilla-Diaz[91], F. Bonini[7], A. Booth[75], F. Boran[41], S. Bordoni[1], R. Borges Merlo[9], A. Borkum[36], N. Bostan[83], J. Bracinik[92], D. Braga[3], B. Brahma[93], D. Brailsford[84], F. Bramati[88], A. Branca[88], A. Brandt[34], J. Bremer[1], C. Brew[94], S. J. Brice[3], V. Brio[64], C. Brizzolari[88,90], C. Bromberg[68], J. Brooke[8], A. Bross[3], G. Brunetti[88,90], M. Brunetti[43], N. Buchanan[67], H. Budd[13], J. Buergi[95], D. Burgardt[96], S. Butchart[36], G. Caceres V.[76], I. Cagnoli[72,73], T. Cai[47], R. Calabrese[25,26], J. Calcutt[97], M. Calin[98], L. Calivers[95], E. Calvo[18], A. Caminata[71], A. F. Camino[99], W. Campanelli[28], A. Campani[71,100], A. Campos Benitez[101], N. Canci[102], J. Capó[20], I. Caracas[103], D. Caratelli[104], D. Carber[67], J. M. Carceller[1], G. Carini[7], B. Carlus[40], M. F. Carneiro[7], P. Carniti[88], I. Caro Terrazas[67], H. Carranza[34], N. Carrara[76], L. Carroll[16], T. Carroll[105], A. Carter[106], E. Casarejos[45], D. Casazza[25], J. F. Castaño Forero[107], F. A. Castaño[108], A. Castillo[109], C. Castromonte[110], E. Catano-Mur[111], C. Cattadori[88], F. Cavalier[37], F. Cavanna[3], S. Centro[112], G. Cerati[3], C. Cerna[113], A. Cervelli[72], A. Cervera Villanueva[20], K. Chakraborty[114], S. Chakraborty[115], M. Chalifour[1], A. Chappell[43], N. Charitonidis[1], A. Chatterjee[114], H. Chen[7], M. Chen[44], W. C. Chen[116], Y. Chen[30], Z. Chen-Wishart[106], D. Cherdack[10], C. Chi[117], R. Chirco[23], N. Chitirasreemadam[62,63], K. Cho[118], S. Choate[85], D. Chokheli[6], P. S. Chong[119], B. Chowdhury[22], D. Christian[3], A. Chukanov[29], M. Chung[120], E. Church[42], M. F. Cicala[53], M. Cicerchia[112], V. Cicero[72,73], R. Ciolini[62], P. Clarke[54], G. Cline[11], T. E. Coan[121], A. G. Cocco[102], J. A. B. Coelho[122], A. Cohen[122], J. Collazo[45], J. Collot[123], E. Conley[124], J. M. Conrad[52], M. Convery[30], S. Copello[71], P. Cova[125,126], C. Cox[106], L. Cremaldi[127], L. Cremonesi[75], J. I. Crespo-Anadón[18], M. Crisler[3], E. Cristaldo[88,66], J. Crnkovic[3], G. Crone[53], R. Cross[43], A. Cudd[14], C. Cuesta[18], Y. Cui[128], F. Curciarello[129], D. Cussans[8], J. Dai[123], O. Dalager[44], R. Dallavalle[122], W. Dallaway[116], H. da Motta[130], Z. A. Dar[111], R. Darby[36], L. Da Silva Peres[131], Q. David[40], G. S. Davies[127], S. Davini[71], J. Dawson[122], R. De Aguiar[9], P. De Almeida[9], P. Debbins[83], I. De Bonis[12], M. P. Decowski[132,133], A. de Gouvêa[134], P. C. De Holanda[9], I. L. De Icaza Astiz[36], P. De Jong[132,133], P. Del Amo Sanchez[12], A. De la Torre[18], G. De Lauretis[40],

Citation: Performance of a modular ton-scale pixel-readout liquid argon time projection chamber. *Instruments* **2024**, *1*, 0. https://doi.org/

Received:
Revised:
Accepted:
Published:

† In memory of our colleague, Dr. Davide Salvatore Porzio, who is no longer with us.

Abstract: The Module-0 Demonstrator is a single-phase 600 kg liquid argon time projection chamber operated as a prototype for the DUNE liquid argon near detector. Based on the ArgonCube design concept, Module-0 features a novel 80k-channel pixelated charge readout and advanced high-coverage photon detection system. In this paper, we present an analysis of an eight-day data set consisting of 25 million cosmic ray events collected in the spring of 2021. We use this sample to demonstrate the imaging performance of the charge and light readout systems as well as the signal correlations between the two. We also report argon purity and detector uniformity measurements, and provide comparisons to detector simulations.

1. Introduction

Charge readout in liquid argon time projection chambers (LArTPCs) has traditionally been accomplished via a set of projective wire planes, as successfully demonstrated e.g. in the ICARUS [1], ArgoNeuT [2], MicroBooNE [3] and ProtoDUNE-SP [4,5] experiments, and as planned for the first large detector module of the DUNE experiment currently in preparation at the Sanford Underground Research Facility (SURF) underground laboratory in South Dakota [6]. However, this approach leads to inherent ambiguities in the 3D reconstruction of charge information that present serious challenges for LArTPC-based near detectors, where a high rate of neutrino interactions and an associated high-intensity muon flux cannot be avoided. In particular, 3D reconstruction becomes limited by overlap of charge clusters in one or more projections, and the unique association of deposited charge to single interactions becomes intractable.

To overcome event pile-up, a novel approach has been proposed and is being developed for the LArTPC of the Near Detector (ND) complex of the DUNE experiment, close to the neutrino source at Fermilab. This technology implements three main innovations compared to traditional wire-based LArTPCs: a pixelated charge readout enabling true 3D reconstruction, a high-performance light readout system providing fast and efficient detection of scintillation light, and segmentation into optically isolated regions. By achieving a low signal occupancy in both readout systems, the segmentation enables efficient reconstruction and unambiguous matching of charge and light signals.

This paper describes the first tonne-scale prototype of this technology, referred to as Module-0, and its performance as evaluated with a large cosmic ray data set acquired over a period of several days at the University of Bern. Section 2 provides an overview of the detector, as well as of its charge and light readout systems. Section 3 discusses the performance of the charge readout system in detail, and Section 4 does the same for the light readout system. Section 5 then reviews several analyses performed with reconstructed tracks from the cosmic ray data set collected during the Module-0 that allow to assess the performance of the fully-integrated system. Important metrics for successful operation are addressed, such as electron lifetime, electric field uniformity, and the ability to match charge and light signals, among others. Section 6 offers some concluding thoughts.

2. The Module-0 Demonstrator

2.1. Detector Description

The Module-0 demonstrator is the first fully integrated, tonne-scale prototype of the DUNE Liquid Argon Near Detector (ND-LAr) design. That detector will consist of a 7×5 array of $1 \times 1 \times 3$ m^3 detector modules [7] based on the ArgonCube detector concept [8], each housing two 50 cm–drift TPC volumes with 24.9% optical detector coverage of the interior area. Module-0 has dimensions of 0.7 m $\times$ 0.7 m $\times$ 1.4 m, and brings together the innovative features of LArPix [9,10] pixelated 3D charge readout, advanced ArCLight [11] and Light Collection Module (LCM) [12] optical detectors, and field shaping provided by a low-profile resistive shell [13]. This integrated prototype also tests the charge and light

Prepared for submission to JINST

Testbeam analysis of biasing structures for irradiated hybrid pixel detectors

C. M. Buttar[a] **Y. Gao**[b] **R. González López**[c] **D. Maneuski**[a] **E. Pender**[b] **Q. Qin**[d] **A. G. Rennie**[e,1,2] **M. Sullivan**[c] **J. T. Taylor**[c] **K. Wraight**[a]

[a] *University of Glasgow*
School of Physics and Astronomy, Kelvin Building, University Avenue, Glasgow, G12 8QQ
[b] *University of Edinburgh*
School of Physics and Astronomy, James Clerk Maxwell Building, Peter Guthrie Tait Road, Edinburgh, EH9 3FD
[c] *University of Liverpool*
Department of Physics, Oliver Lodge, Oxford Street, Liverpool, L69 7ZE
[d] *University of Manchester*
Department of Physics and Astronomy, Schuster Building, Oxford Road, Manchester, M13 9PL
[e] *University of California, Irvine*
Department of Physics and Astronomy, 4129 Frederick Reines Hall, Irvine, CA 92697-4575

E-mail: adam.rennie@cern.ch

Abstract: Following the Phase-II upgrade during Long Shutdown (LS3), the LHC aims to reach a peak instantaneous luminosity of 7.5×10^{34} cm^{-2} s^{-1}, which corresponds to an average of around 200 inelastic proton-proton collisions per beam-crossing (every 25 ns). To cope with these conditions, the ATLAS Inner Detector will be replaced by a new all-silicon system — the Inner Tracker (ITk). The ITk will be operational for more than ten years, during which time ATLAS is expected to record approximately 4000 fb^{-1} of data. The ITk's pixel sub-system is based on hybrid pixel modules with new silicon sensors and readout chips. These studies focus on testbeam campaigns undertaken to study the spatial resolution and efficiencies of hybrid pixel detector modules based on the first large-structure prototype front-end readout chip — the RD53A — using planar silicon sensors. These devices have been irradiated to replicate the effect of the high radiation environment present during operation in the ATLAS detector. Results for devices using sensors with different punch-through bias structures and using different readout chips are summarised. Those with sensors incorporating a punch-through bias structure are found to exhibit systematically lower efficiency than those without, as a result of local areas of relative inefficiency around the punch-through dots. Despite this, all devices measured are found to satisfy the requirement of 97% efficiency at $V_{\text{bias}} = 400$ V after being irradiated to end-of-life fluence.

Keywords: Hybrid detectors, Radiation-hard detectors, Particle tracking detectors (Solid-state detectors), Performance of High Energy Physics Detectors

[1] Corresponding author.
[2] Previously at University of Glasgow, School of Physics and Astronomy, Kelvin Building, University Avenue, Glasgow, G12 8QQ.

Prepared for submission to JINST

Front-end electronics development of large-area SiPM arrays for high-precision single-photon time measurement

W. Zhi[a] **, J.N. Tang**[a] **, M.X. Wang**[a] **, Y.Q. Tan**[a] **, W.H. Wu**[a,1] **and D.L. Xu**[a,b]

[a] *School of Physics and Astronomy, Shanghai Jiao Tong University*
800 Dongchuan Rd, Minhang District, Shanghai, China
[b] *Tsung-Dao Lee Institute, Shanghai Jiao Tong Univeristy*
520 Shengrong Rd, Pudong New Area, Shanghai, China

E-mail: wuweihao@sjtu.edu.cn

Abstract: TRopIcal DEep-sea Neutrino Telescope (TRIDENT) plans to incorporate silicon photomultipliers (SiPMs) with superior time resolution in addition to photomultiplier tubes (PMTs) into its detection units, namely hybrid Optical Digital Modules (hDOMs), to improve its angular resolution. However, the time resolution significantly degrades for large-area SiPMs due to the increased parasitic capacitance, posing significant challenges for the readout electronics of SiPMs in hDOM. We designed the front-end readout electronics for large-area SiPM arrays dedicated to high-precision time measurements, which consists of a high-speed pre-amplifier based on transformers (MABA-007159) and radio frequency (RF) amplifiers (BGA2803), a series-parallel combination SiPM array with reduced capacitance, and an analog multi-channel summing circuit. We measured the single photon time resolution (SPTR) of a 4×4 SiPM (Hamamatsu S13360-3050PE) array (12×12 mm^2) of approximately 300 ps FWHM with a power consumption of less than 100 mW. This front-end readout design enables the large-area SiPM array to achieve high-precision SPTR with low power consumption.

Keywords: Neutrino detectors; Photon detectors for UV, visible and IR photons (solid-state); Front-end electronics for detector readout; Analogue electronic circuits

[1] Corresponding author.

Numerical simulation of charging up, accumulation of space charge and formation of discharges

Purba Bhattacharya[a], Promita Roy[b], Tanay Dey[c], Jaydeep Datta[d], Prasant K. Rout[e], Nayana Majumdar[f], Supratik Mukhopadhyay[g]

[a]*Department of Physics, School of Basic and Applied Sciences, Adamas University, Kolkata, Inda*
[b]*Department of Physics, , Virginia Polytechnic Institute & State University, VA, United States*
[c]*School of Physical Sciences, National Institute for Science Education and Research, Jatni, Khurda, Odisha, India*
[d]*Center for Frontiers in Nuclear Science, Department of Physics and Astronomy, Stony Brook University, 100 Nicolls Road, Stony Brook, New York, 11794, USA*
[e]*National Central University, Taoyuan City, Taiwan*
[f]*Applied Nuclear Physics Division, Saha Institute of Nuclear Physics, Kolkata, India*
[g]*Retired from Applied Nuclear Physics Division, Saha Institute of Nuclear Physics, Kolkata, India*

Abstract

Aging and stability of gaseous ionization detectors are intricately related to charging up, accumulation of space charge and formation of discharges. All these phenomena, in their turn, depend on the dynamics of charged particles within the device. Because of the large number of particles involved and their complex interactions, the dynamic processes of generation and loss of charged particles, and their transport within the detector volume are extremely expensive to simulate numerically. In this work, we propose and evaluate possible algorithms / approaches that show some promise in relation to the above-mentioned problems. Several important ionization detectors having parallel plate configurations, such as GEM, Micromegas, RPCs and THGEMs, are considered for this purpose. Information related to primary ionization is obtained from HEED, while all the transport properties are evaluated using MAGBOLTZ. The transport dynamics have been followed using two different approaches. In one, particle description using neBEM-Garfield++ combination has been used. For this purpose, the neBEM solver has been significantly improved such that perturbations due to the charged particles present within the device are considered while estimating electric field. In the other approach, the transport is simulated following hydrodynamic model using COMSOL during which the electric field is also provided by COMSOL where it is easy to set up space charge effects. A comparison between these possible approaches will be presented. Effect of different simulation parameters will also be demonstrated using simple examples.

Keywords: Gaseous detector, Aging, Stability, Space charge, Charging up, Discharge, Simulation,

1. Introduction

Charging up is a phenomena commonly observed in gaseous detectors having dielectric materials exposed to the active volume of gas mixture where primaries and secondaries are generated, and electron multiplication occurs. They can affect long-term stability of a detector and lead to response non-uniformity [1]. Space charge accumulation occurs in gaseous detectors due to the presence of charged particles within the active gas volume before they are collected at suitable electrodes. Existence of space charge can distort the applied electric field configuration, make detector response non-uniform and unstable, and has the potential to lead to discharges [2], affecting detector performance significantly. Besides making a detector lose its stability in the immediate time scale, formation of discharges has the capability of accelerating detector aging and damaging it for good. Thus, it is important to understand these phenomena using both experimental and numerical tools. However, these topics, and the associated discharge formation process, are com-

Email address: purba.bhattacharya85@gmail.com (Purba Bhattacharya)

Probabilistic assessment of the reactor vessel lifetime

V. V. Ryazanov

Institute for Nuclear Research, pr. Nauki, 47 Kiev, Ukraine, e-mail: vryazan19@gmail.com

Highlights

- A simple and rapid method for assessing neutron irradiation on a reactor vessel is proposed
- Queuing theory is used to estimate the lifetime of the reactor vessel walls
- The behavior of radiation defects is modeled by a random process of death and birth
- For assessments, information about neutron fluence and fast neutron energy is needed

Abstract

A simple and rapid method is proposed for assessing the reduction in the lifetime of steel walls of the reactor vessel under neutron irradiation. The method is based on modeling the number of radiation defects by the behavior of a general time-dependent random process of death and birth and queuing theory. Necessary data for assessments: the estimated operating time of the reactor (in years), the actual operating time of the reactor, the accumulated fluence depending on time, the temperature on the walls of the reactor vessel, the neutron absorption cross section of the steel of the reactor walls, the energy of fast neutrons striking the walls. The main problem: getting this accurate data.
Keywords: neutron irradiation, reactor vessel lifetime, process of death and birth

1. Introduction

The impact of neutron irradiation on the duration of the steady state of the walls of the reactor vessel (RV) is one of the main issues in nuclear energy. The safety and reliability of the operation of a nuclear power plant are associated with the reliability of predicting changes in the viscosity characteristics of the reactor vessel material. This problem is presented in detail in many studies [1-32]; it is associated with issues of safe operation of the reactor, extending the life of the reactor, and many other tasks. The procedure usually performed when considering problems of this kind is to measure the dependence of the change in the shift of the critical brittleness temperature (or radiation embrittlement coefficient) on the temperature of the witness samples.

Thus, a large amount of data was accumulated on the radiation embrittlement of low-alloy vessel steels, on the relationship between the critical temperature of embrittlement and the resulting fluence, and on other aspects of the problem under consideration, which was then used in predicting changes in the lifetime of RV materials. Probabilistic approaches to solving this problem have been considered; recent works have used Bayesian methods, approaches related to machine learning, etc.

This article proposes a simplified probabilistic approach to solving the problem of changing the lifetime of the walls of the RV under the influence of irradiation. This is an integral approach that does not take into account many details that do not have a decisive influence on the final result. As in experimental work, the influence of neutron fluence is considered important. Lattice atoms directly displaced by incident particles are defined as a primary knocked-out atom (PKA). PVAs have an energy spectrum even in the case of monochromatic irradiation; their energy varies from zero to a certain maximum value M_{max}. Getting into a solid body, a fast particle is involved in a complex process of interaction with electrons and atomic nuclei in the crystal lattice. The statistical approach is based on determining the probability of the interaction process occurring. The emerging defects in the crystal lattice and crystalline crystals are considered as a statistical system, subject to the general laws of the theory of random processes, statistical physics and nonequilibrium thermodynamics. It is assumed that at

An Experimentally Benchmarked Geant4 SiPM-Based Scintillator Detector Simulation Platform for Gamma Ray Detection

Lysander Miller[a], Airlie Chapman[a], Katie Auchettl[b], Jeremy M. C. Brown[c]

[a]*Department of Mechanical Engineering, The University of Melbourne, Parkville, VIC 3010, Australia*
[b]*School of Physics, The University of Melbourne, Parkville, VIC 3010, Australia*
[c]*Optical Sciences Centre, Department of Physics and Astronomy, Swinburne University of Technology, Hawthorn, VIC 3122, Australia*

Abstract

Radiation detection is vital for naturally occurring radioactive material detection, port and border monitoring, and homeland security operations. SiPM-based single-volume scintillator detectors offer a cost-effective and robust solution that enables timely radioactive site surveys, while retaining accuracy and sensitivity sufficient for isotope identification. Enhanced site surveying can be achieved by optimising scintillator detector design. In this work, a detailed GAGG:Ce, CLLBC:Ce, BGO, NaI:Tl, and CsI:Tl SiPM-based scintillator detector simulation platform was developed with the Monte Carlo radiation transport toolkit, Geant4, and experimentally benchmarked. This simulation platform successfully predicted the spectral features for selected gamma ray emitting isotopes with energies between 30 keV to 2 MeV. The full width half maximum (FWHM) and normalised cross-correlation coefficient (NCCC) between simulated and experimental energy spectra were also compared. The majority of simulated FWHM values reproduced the experimental results within 2% and the NCCC values demonstrated agreement between the simulated and experimental energy spectra. Discrepancies in these figures of merit can be attributed to detector signal processing electronics modelling, geometry approximations, and multiple Compton scattering within the detector and surrounding environment.

Keywords: GAGG, CLLBC, BGO, NaI, CsI, Geant4 optical physics

1. Introduction

Uncontrolled radiological and nuclear (R&N) material dispersion pose a significant threat to civil and military environments [1, 2, 3]. Radiation detection capabilities play an important role in large-area R&N surveying as they provide first responders with prompt situational awareness. Recent developments in new scintillator crystals, such as CLLBC:Ce [4, 5], and silicon photomultiplier (SiPM) technology allow for compact, lightweight, and rugged detectors that are suitable for large-area radiation detection. An important aspect of detector design is optimising the scintillator geometry and material for accurate radiation measurements given different R&N surveying modalities

Microscopic parametrization of the near threshold oscillations of the nucleon time-like effective electromagnetic form factors

Francesco Rosini* and Simone Pacetti
Dipartimento di Fisica e Geologia, INFN Sezione di Perugia, 06123 Perugia, Italy

Olga Shekhovtsova
INFN Sezione di Perugia, 06123 Perugia, Italy and
National Science Centre, Kharkov Institute of Physics and Technology, Akademicheskaya, Ukraine

Egle Tomasi-Gustafsson
DPhN, IRFU, CEA, Université Paris-Saclay, 91191 Gif-sur-Yvette Cedex, France

We present an analysis of the recent near threshold BESIII data for the nucleon time-like effective form factors. The damped oscillation emerging from the subtraction of the dipole formula is treated in non-perturbative-QCD, making use of the light cone distribution amplitudes expansion. Non-perturbative effects are accounted for by considering Q^2-dependent coefficients in such expansions, whose free parameters are determined by fitting to the proton and neutron data. Possible implications and future analysis have been discussed.

I. INTRODUCTION

The theoretical impossibility of describing the nucleon internal structure in terms of strongly interacting quarks and gluons, which are the fundamental fields of quantum chromodynamics, enhances the electromagnetic form factors (EMFFs) to the role of unique and privileged tools to unravel the dynamics underlying the electromagnetic interaction of nucleons. They provide the most effective description of the mechanisms that determine and rule the dynamic and static properties of nucleons. In specific reference frames, EMFFs represent the Fourier transforms of spatial charge and magnetic momentum densities.

Recently, the BESIII [1] experiment measured the time-like nucleon form factors (FFs) at center-of-mass energies between 2.0 GeV and 3.5 GeV [2–6]. These data present an oscillating behavior [7–12], which manifests itself as a periodic, exponentially dumped component over the typical dipolar carrier, usually identified as the only contribution. The nature of such an oscillating component is still unknown. Possible explanations rely either on the final state interaction between the baryon and the antibaryon, or in a phenomenon intrinsic to the baryon structure. In the latter case, the invoked phenomenon would be encoded by the EMFFs of nucleons.

In order to investigate this eventuality we propose a parametrization for the EMFFs defined by considering the nucleons as triplets of collinear quarks lying at light-like distances in the light-front framework [13].

The matrix element of the "+" component of the hadronic current J^μ, which depends directly on the EMFFs, evaluated between the baryon and antibaryon particle states, can then be expanded using the Lorentz invariance of the three quark Fock state's matrix elements.

The resulting form depends on a set of functions of the four momentum squared fractions, called light cone distribution amplitudes (LCDAs), and a deep knowledge of their expression can provide further information about the form factors shape. Using the $\mathcal{L}_{\rm QCD}$ conformal symmetry [14], the LCDAs are expanded on a polynomial basis, the most common choice being represented by the orthonormal Appell polynomials, defined on the triangle $T(x_1, x_3) = \{(x_1, x_3) \in \mathbb{R} : x_1 > 0, x_3 > 0, x_1 + x_3 < 1\}$, where $x_i = k_i^+/P^+$ are the quark's light front momentum fractions along is the $(^+)$ direction and so the following relation holds: $\sum_{i=1}^{3} x_i = 1$. The only unknown quantities now are the expansion coefficients, which have to be determined considering the phenomenology of the problem. The nonperturbative coefficients admit an evolution equation in the conformal symmetry framework, and their values can be determined theoretically by QCD sum rules. On the other hand, we are considering a center of mass energy of the system between 2.0 GeV and 3.5 GeV, so we are not allowed to use perturbative methods. What we propose then is to perform a truncated Laurent expansion of the non-perturbative coefficients over the negative powers of the four momentum squared, subsequently performing a fit over the recent BESIII experimental data to determine these coefficients. The final goal of this description is to find whether the oscillations of the EMFFs can be described by the model functions.

II. THE MICROSCOPIC MODEL

One of the most effective ways to describe subnuclear processes is to work on a light front framework, expanding the involved particle states in a free particle state basis, commonly known as Fock states. For a baryon we

* francesco.rosini@studenti.unipg.it

Rare B and K decays in a scotogenic model

Chuan-Hung Chen[1, 2, *] and Cheng-Wei Chiang[3, 2, †]

[1]*Department of Physics, National Cheng-Kung University, Tainan 70101, Taiwan*

[2]*Physics Division, National Center for Theoretical Sciences, Taipei 10617, Taiwan*

[3]*Department of Physics and Center for Theoretical Physics, National Taiwan University, Taipei 10617, Taiwan*

(Dated: March 6, 2024)

Abstract

A scotogenic model can radiatively generate the observed neutrino mass, provide a dark matter candidate, and lead to rare lepton flavor-violating processes. We aim to extend the model to establish a potential connection to the quark flavor-related processes within the framework of scotogenesis, enhancing the unexpectedly large branching ratio (BR) of $B^+ \to K^+\nu\bar{\nu}$, observed by Belle II Collaboration. Meanwhile, the model can address tensions between some experimental measurements and standard model (SM) predictions in flavor physics, such as the muon $g-2$ excess and the higher BR of $B_s \to \mu^-\mu^+$. We introduce in the model the following dark particles: a neutral singlet Dirac-type lepton (N); two inert Higgs doublets ($\eta_{1,2}$), with one of which carrying a lepton number; a charged singlet dark scalar (χ^+), and a singlet vector-like up-type dark quark (T). The first two entities are responsible for the radiative neutrino mass, and χ^+ couples to right-handed quarks and leptons and can resolve the tensions existing in muon $g-2$ and $B_s \to \mu^-\mu^+$. Furthermore, the BR of $B^+ \to K^+\nu\bar{\nu}$ can be enhanced up to a factor of 2 compared to the SM prediction through the mediations of the dark T and the charged scalars. In addition, we also study the impacts on the $K \to \pi\nu\bar{\nu}$ decays.

*E-mail: physchen@mail.ncku.edu.tw

†E-mail: chengwei@phys.ntu.edu.tw

Macroscopic neutrinoless double beta decay: long range quantum coherence

Gordon Baym and Jen-Chieh Peng
Illinois Center for Advanced Studies of the Universe
and Department of Physics, University of Illinois, 1110 W. Green Street, Urbana, IL 61801

(Dated: March 6, 2024)

We introduce the concept of "macroscopic neutrinoless double beta decay" (MDBD) for Majorana neutrinos. In this process an antineutrino produced by a nucleus undergoing beta decay, $X \to Y + e^- + \bar{\nu}_e$, is absorbed as a neutrino by another identical X nucleus via the inverse beta decay reaction, $\nu_e + X \to e^- + Y$. The distinct signature of MDBD is that the total kinetic energy of the two electrons equals twice the endpoint energy of single beta decay. The amplitude for MDBD, a coherent sum over the contribution of different mass states of the intermediate neutrinos, reflects quantum coherence over macroscopic distances, and is a new macroscopic quantum effect. We evaluate the rate of MDBD for a macroscopic sample of "X" material, e.g., tritium, acting both as the source and the target. The accidental background for MDBD originating from two separate single beta decays, which contains two final state neutrinos, can be readily rejected by measuring the energy of the detected two electrons. We discuss the similarities and differences between the MDBD and conventional neutrinoless double beta decay.

PACS numbers:

I. INTRODUCTION

The neutrino, if a Majorana rather than a Dirac fermion, would be its own antiparticle. A key experimental signature distinguishing Majorana neutrinos from Dirac neutrinos is nuclear neutrinoless double beta decay (0νDBD),

$$(A, Z) \to (A, Z+2) + e^- + e^-. \tag{1}$$

Despite the importance of determining whether neutrinos are Majorana or Dirac, and despite a major experimental effort, only upper limits for 0νDBD have so far been obtained [1–3]. Ongoing and future experiments with multi-ton detectors will further improve the sensitivity in these searches [4].

The existence of a Majorana neutrino implies lepton-number non-conservation, hence physics beyond the Standard Model. Majorana neutrinos have only two spin states: when massless the left-handed state is a neutrino and the right-handed an antineutrino. The "sea-saw" mechanism for Majorana neutrinos can then provide a natural explanation for the very light neutrino masses inferred from tritium beta decay (TBD) and neutrino oscillation experiments [5].

The standard picture of neutrinoless double beta decay is that the *antineutrino* emitted from a neutron in a nucleus is absorbed as a *neutrino* on a neutron in the same nucleus. But there is in general no requirement in neutrinoless double beta decay that the second neutron be in the same nucleus (or indeed that the second nucleus be the same nuclide as the first, or even that the two down quarks undergoing weak interactions be in different neutrons). In this paper, we introduce the concept of "macroscopic neutrinoless double beta decay" (MDBD), in which a Majorana neutrino emitted from one nucleus is absorbed in a second nucleus. For example, in the single beta decay (XBD) from parent nucleus $X = (A, Z)$ to daughter nucleus $Y = (A, Z+1)$,

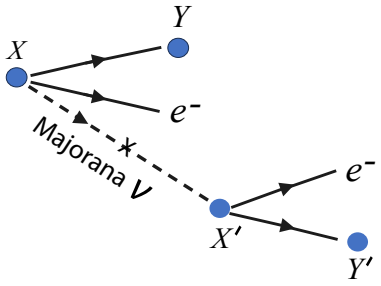

FIG. 1: Illustration of macroscopic neutrinoless double beta decay, with time running to the right. The first nucleus, X undergoes a beta decay emitting an electron and a Majorana antineutrino, which is absorbed as a neutrino by a second nucleus X' in an inverse beta decay. The sum of the energies of the two electron emitted is just the sum of the individual endpoint energies in the beta decays of X and X'.

$$X \to Y + e^- + \bar{\nu}_e, \tag{2}$$

the antineutrino produced is, for Dirac type neutrinos, distinct from ν_e and cannot participate in the inverse beta decay (IXBD) reaction

$$\nu_e + X \to e^- + Y; \tag{3}$$

the nucleus X can only absorb an electron neutrino, ν_e, to reach the final state $e^- + Y$. If neutrinos are Majorana however, then the neutrino and antineutrino are not distinct particles, and the antineutrino in the XBD can then participate in the IXBD. The combination of these

Observation of Seven Astrophysical Tau Neutrino Candidates with IceCube

R. Abbasi,[17] M. Ackermann,[63] J. Adams,[18] S. K. Agarwalla,[40,*] J. A. Aguilar,[12] M. Ahlers,[22] J.M. Alameddine,[23] N. M. Amin,[44] K. Andeen,[42] G. Anton,[26] C. Argüelles,[14] Y. Ashida,[53] S. Athanasiadou,[63] S. N. Axani,[44] X. Bai,[50] A. Balagopal V.,[40] M. Baricevic,[40] S. W. Barwick,[30] V. Basu,[40] R. Bay,[8] J. J. Beatty,[20,21] J. Becker Tjus,[11,†] J. Beise,[61] C. Bellenghi,[27] C. Benning,[1] S. BenZvi,[52] D. Berley,[19] E. Bernardini,[48] D. Z. Besson,[36] E. Blaufuss,[19] S. Blot,[63] F. Bontempo,[31] J. Y. Book,[14] C. Boscolo Meneguolo,[48] S. Böser,[41] O. Botner,[61] J. Böttcher,[1] E. Bourbeau,[22] J. Braun,[40] B. Brinson,[6] J. Brostean-Kaiser,[63] R. T. Burley,[2] R. S. Busse,[43] D. Butterfield,[40] M. A. Campana,[49] K. Carloni,[14] E. G. Carnie-Bronca,[2] S. Chattopadhyay,[40,*] N. Chau,[12] C. Chen,[6] Z. Chen,[55] D. Chirkin,[40] S. Choi,[56] B. A. Clark,[19] L. Classen,[43] A. Coleman,[61] G. H. Collin,[15] A. Connolly,[20,21] J. M. Conrad,[15] P. Coppin,[13] P. Correa,[13] D. F. Cowen,[59,60] P. Dave,[6] C. De Clercq,[13] J. J. DeLaunay,[58] D. Delgado,[14] S. Deng,[1] K. Deoskar,[54] A. Desai,[40] P. Desiati,[40] K. D. de Vries,[13] G. de Wasseige,[37] T. DeYoung,[24] A. Diaz,[15] J. C. Díaz-Vélez,[40] M. Dittmer,[43] A. Domi,[26] H. Dujmovic,[40] M. A. DuVernois,[40] T. Ehrhardt,[41] P. Eller,[27] E. Ellinger,[62] S. El Mentawi,[1] D. Elsässer,[23] R. Engel,[31,32] H. Erpenbeck,[40] J. Evans,[19] P. A. Evenson,[44] K. L. Fan,[19] K. Fang,[40] K. Farrag,[16] A. R. Fazely,[7] N. Feigl,[10] S. Fiedlschuster,[26] A. T. Fienberg,[60] C. Finley,[54] L. Fischer,[63] D. Fox,[59] A. Franckowiak,[11] A. Fritz,[41] P. Fürst,[1] J. Gallagher,[39] E. Ganster,[1] A. Garcia,[14] L. Gerhardt,[9] A. Ghadimi,[58] C. Glaser,[61] T. Glauch,[27] T. Glüsenkamp,[26,61] N. Goehlke,[32] J. G. Gonzalez,[44] S. Goswami,[58] D. Grant,[24] S. J. Gray,[19] O. Gries,[1] S. Griffin,[40] S. Griswold,[52] K. M. Groth,[22] C. Günther,[1] P. Gutjahr,[23] C. Haack,[26] A. Hallgren,[61] R. Halliday,[24] L. Halve,[1] F. Halzen,[40] H. Hamdaoui,[55] M. Ha Minh,[27] K. Hanson,[40] J. Hardin,[15] A. A. Harnisch,[24] P. Hatch,[33] A. Haungs,[31] K. Helbing,[62] J. Hellrung,[11] F. Henningsen,[27] L. Heuermann,[1] N. Heyer,[61] S. Hickford,[62] A. Hidvegi,[54] C. Hill,[16] G. C. Hill,[2] K. D. Hoffman,[19] S. Hori,[40] K. Hoshina,[40,‡] W. Hou,[31] T. Huber,[31] K. Hultqvist,[54] M. Hünnefeld,[23] R. Hussain,[40] K. Hymon,[23] S. In,[56] A. Ishihara,[16] M. Jacquart,[40] O. Janik,[1] M. Jansson,[54] G. S. Japaridze,[5] M. Jeong,[56] M. Jin,[14] B. J. P. Jones,[4] D. Kang,[31] W. Kang,[56] X. Kang,[49] A. Kappes,[43] D. Kappesser,[41] L. Kardum,[23] T. Karg,[63] M. Karl,[27] A. Karle,[40] U. Katz,[26] M. Kauer,[40] J. L. Kelley,[40] A. Khatee Zathul,[40] A. Kheirandish,[34,35] J. Kiryluk,[55] S. R. Klein,[8,9] A. Kochocki,[24] R. Koirala,[44] H. Kolanoski,[10] T. Kontrimas,[27] L. Köpke,[41] C. Kopper,[26] D. J. Koskinen,[22] P. Koundal,[31] M. Kovacevich,[49] M. Kowalski,[10,63] T. Kozynets,[22] J. Krishnamoorthi,[40,*] K. Kruiswijk,[37] E. Krupczak,[24] A. Kumar,[63] E. Kun,[11] N. Kurahashi,[49] N. Lad,[63] C. Lagunas Gualda,[63] M. Lamoureux,[37] M. J. Larson,[19] S. Latseva,[1] F. Lauber,[62] J. P. Lazar,[14,40] J. W. Lee,[56] K. Leonard DeHolton,[60] A. Leszczyńska,[44] M. Lincetto,[11] Q. R. Liu,[40] M. Liubarska,[25] E. Lohfink,[41] C. Love,[49] C. J. Lozano Mariscal,[43] F. Lucarelli,[28] W. Luszczak,[20,21] Y. Lyu,[8,9] J. Madsen,[40] K. B. M. Mahn,[24] Y. Makino,[40] E. Manao,[27] S. Mancina,[40,48] W. Marie Sainte,[40] I. C. Mariş,[12] S. Marka,[46] Z. Marka,[46] M. Marsee,[58] I. Martinez-Soler,[14] R. Maruyama,[45] F. Mayhew,[24] T. McElroy,[25] F. McNally,[38] J. V. Mead,[22] K. Meagher,[40] S. Mechbal,[63] A. Medina,[21] M. Meier,[16] Y. Merckx,[13] L. Merten,[11] J. Micallef,[24] J. Mitchell,[7] T. Montaruli,[28] R. W. Moore,[25] Y. Morii,[16] R. Morse,[40] M. Moulai,[40] T. Mukherjee,[31] R. Naab,[63] R. Nagai,[16] M. Nakos,[40] U. Naumann,[62] J. Necker,[63] A. Negi,[4] M. Neumann,[43] H. Niederhausen,[24] M. U. Nisa,[24] A. Noell,[1] A. Novikov,[44] S. C. Nowicki,[24] A. Obertacke Pollmann,[16] V. O'Dell,[40] M. Oehler,[31] B. Oeyen,[29] A. Olivas,[19] R. Orsoe,[27] J. Osborn,[40] E. O'Sullivan,[61] H. Pandya,[44] D. V. Pankova,[60] N. Park,[33] G. K. Parker,[4] E. N. Paudel,[44] L. Paul,[42,50] C. Pérez de los Heros,[61] J. Peterson,[40] S. Philippen,[1] A. Pizzuto,[40] M. Plum,[50] A. Pontén,[61] Y. Popovych,[41] M. Prado Rodriguez,[40] B. Pries,[24] R. Procter-Murphy,[19] G. T. Przybylski,[9] C. Raab,[37] J. Rack-Helleis,[41] K. Rawlins,[3] Z. Rechav,[40] A. Rehman,[44] P. Reichherzer,[11] G. Renzi,[12] E. Resconi,[27] S. Reusch,[63] W. Rhode,[23] B. Riedel,[40] A. Rifaie,[1] E. J. Roberts,[2] S. Robertson,[8,9] S. Rodan,[56] G. Roellinghoff,[56] M. Rongen,[26] C. Rott,[53,56] T. Ruhe,[23] L. Ruohan,[27] D. Ryckbosch,[29] I. Safa,[14,40] J. Saffer,[32] D. Salazar-Gallegos,[24] P. Sampathkumar,[31] S. E. Sanchez Herrera,[24] A. Sandrock,[62] M. Santander,[58] S. Sarkar,[25] S. Sarkar,[47] J. Savelberg,[1] P. Savina,[40] M. Schaufel,[1] H. Schieler,[31] S. Schindler,[26] L. Schlickmann,[1] B. Schlüter,[43] F. Schlüter,[12] N. Schmeisser,[62] T. Schmidt,[19] J. Schneider,[26] F. G. Schröder,[31,44] L. Schumacher,[26] G. Schwefer,[1] S. Sclafani,[19] D. Seckel,[44] M. Seikh,[36] S. Seunarine,[51] R. Shah,[49] A. Sharma,[61] S. Shefali,[32] N. Shimizu,[16] M. Silva,[40] B. Skrzypek,[14] B. Smithers,[4] R. Snihur,[40] J. Soedingrekso,[23] A. Søgaard,[22] D. Soldin,[32] P. Soldin,[1] G. Sommani,[11] C. Spannfellner,[27] G. M. Spiczak,[51] M. Stamatikos,[21] T. Stanev,[44] T. Stezelberger,[9] T. Stürwald,[62] T. Stuttard,[22] G. W. Sullivan,[19] I. Taboada,[6] S. Ter-Antonyan,[7] M. Thiesmeyer,[1] W. G. Thompson,[14] J. Thwaites,[40] S. Tilav,[44] K. Tollefson,[24] C. Tönnis,[56] S. Toscano,[12] D. Tosi,[40] A. Trettin,[63] C. F. Tung,[6] R. Turcotte,[31] J. P. Twagirayezu,[24] B. Ty,[40] M. A. Unland Elorrieta,[43] A. K. Upadhyay,[40,*] K. Upshaw,[7] N. Valtonen-Mattila,[61] J. Vandenbroucke,[40] N. van Eijndhoven,[13] D. Vannerom,[15] J. van Santen,[63] J. Vara,[43] J. Veitch-Michaelis,[40] M. Venugopal,[31] M. Vereecken,[37] S.

[47] *Dept. of Physics, University of Oxford, Parks Road, Oxford OX1 3PU, United Kingdom*
[48] *Dipartimento di Fisica e Astronomia Galileo Galilei, Università Degli Studi di Padova, 35122 Padova PD, Italy*
[49] *Dept. of Physics, Drexel University, 3141 Chestnut Street, Philadelphia, PA 19104, USA*
[50] *Physics Department, South Dakota School of Mines and Technology, Rapid City, SD 57701, USA*
[51] *Dept. of Physics, University of Wisconsin, River Falls, WI 54022, USA*
[52] *Dept. of Physics and Astronomy, University of Rochester, Rochester, NY 14627, USA*
[53] *Department of Physics and Astronomy, University of Utah, Salt Lake City, UT 84112, USA*
[54] *Oskar Klein Centre and Dept. of Physics, Stockholm University, SE-10691 Stockholm, Sweden*
[55] *Dept. of Physics and Astronomy, Stony Brook University, Stony Brook, NY 11794-3800, USA*
[56] *Dept. of Physics, Sungkyunkwan University, Suwon 16419, Korea*
[57] *Institute of Physics, Academia Sinica, Taipei, 11529, Taiwan*
[58] *Dept. of Physics and Astronomy, University of Alabama, Tuscaloosa, AL 35487, USA*
[59] *Dept. of Astronomy and Astrophysics, Pennsylvania State University, University Park, PA 16802, USA*
[60] *Dept. of Physics, Pennsylvania State University, University Park, PA 16802, USA*
[61] *Dept. of Physics and Astronomy, Uppsala University, Box 516, S-75120 Uppsala, Sweden*
[62] *Dept. of Physics, University of Wuppertal, D-42119 Wuppertal, Germany*
[63] *Deutsches Elektronen-Synchrotron DESY, Platanenallee 6, 15738 Zeuthen, Germany*

We report on a measurement of astrophysical tau neutrinos with 9.7 years of IceCube data. Using convolutional neural networks trained on images derived from simulated events, seven candidate ν_τ events were found with visible energies ranging from roughly 20 TeV to 1 PeV and a median expected parent ν_τ energy of about 200 TeV. Considering backgrounds from astrophysical and atmospheric neutrinos, and muons from $\pi^\pm/K^\pm$ decays in atmospheric air showers, we obtain a total estimated background of about 0.5 events, dominated by non-ν_τ astrophysical neutrinos. Thus, we rule out the absence of astrophysical ν_τ at the 5σ level. The measured astrophysical ν_τ flux is consistent with expectations based on previously published IceCube astrophysical neutrino flux measurements and neutrino oscillations.

In 2013 IceCube discovered a flux of neutrinos of astrophysical origin [1–3]. The astrophysical neutrino ($\nu^{\rm astro}$) flux normalization and index γ carry information about neutrino sources and their environments [4–15]. Different $\nu^{\rm astro}$ production mechanisms lead to different $\nu_e:\nu_\mu:\nu_\tau$ ratios at the sources but, after standard neutrino oscillations over astrophysical distances, detectable numbers of all three neutrino flavors are expected at Earth [16–24]. Previous measurements at lower energies, using neutrinos produced at accelerators and in the atmosphere ($\nu^{\rm atm}$), have detected ν_τ produced directly [25] and through neutrino oscillations [26–28]. At the much higher energies accessible to this analysis, $\nu_\tau^{\rm atm}$ are strongly suppressed relative to $\nu_\tau^{\rm astro}$ [29], while an unexpected level of presence of $\nu_\tau^{\rm astro}$ in the $\nu^{\rm astro}$ flux could be an indication of new physics [30–43].

Previous analyses [44–47] by IceCube to detect $\nu_\tau^{\rm astro}$ included searches for double-cascade signatures, such as the distinctive "double bang" [16] in the full detector or "double pulse" (DP) waveforms in one or two individual photosensors. The DP signature is produced by the distinct arrival times of light signals at one or more photosensors from the ν_τ interaction and τ decay vertices. IceCube previously observed two candidate $\nu_\tau^{\rm astro}$, ruling out the null hypothesis of no $\nu_\tau^{\rm astro}$ at 2.8σ [46]. The analysis presented in this Letter reports on the low-background, high-significance detection of seven $\nu_\tau^{\rm astro}$ candidate events through the use of convolutional neural networks (CNNs).

IceCube [48] is a neutrino observatory with 5160 Digital Optical Modules (DOMs) on 86 strings [48, 49] in a cubic kilometer of ice at the South Pole. Charged particles produced in neutrino interactions emit Cherenkov light [50] while propagating through the ice; photomultiplier tubes in the DOMs convert this light into electrical pulses that are digitized *in situ*. Light is deposited in the detector in several distinct patterns: long tracks, single cascades, and double cascades. Tracks are produced by muons from, *e.g.*, ν_μ charged-current (CC) interactions, and can start or end inside, or pass through, the detector. Single cascades arise from electromagnetic and/or hadronic particle showers produced by deep inelastic neutrino-nucleon interactions in or near the detector, or by $\overline{\nu}_e$ via the Glashow Resonance [51, 52]. Double cascades are formed by high-energy $\nu_{\tau,\,\rm CC}$ interactions in or near the detector that produce a hadronic shower and a τ lepton at the interaction vertex, followed by a second electromagnetic or hadronic shower at the τ decay vertex (BR$[\tau \to (e,h)] \simeq 83\%$). With a decay length of ~ 50 m/PeV, the τ can travel a macroscopic distance in the ice. For ν_τ energies satisfying $E_{\nu_\tau} \gtrsim 1$ PeV and favorable geometric containment, the double-bang signature can be created, with two energetic and well-separated cascades. Such events are intrinsically rare. In contrast, for lower E_{ν_τ} between roughly 50 TeV $-$ 1 PeV, the ν_τ flux is expected to be higher but in CC interactions the two cascades are closer together. Two cascades as close as about 10 m can produce distinctive patterns correlated across multiple DOMs and strings as the light from each cascade passes by, as well as DP waveforms in one

MAX-PLANCK-MEDAILLE

Expedition to the Zeptouniverse

Flavour experiments promise insights into energy scales as high as 200 TeV and distances as small as 10^{-21} meter and offer the chance to identify New Physics.

Andrzej J. Buras

The Large Hadron Collider (LHC) at CERN will directly probe distance scales as short as 10^{-19} m, corresponding to energy scales at the level of a few TeV. Presently, higher resolution can only be achieved with the help of quantum fluctuations caused by new particles and new forces that act at very short distance scales and modify the predictions of the Standard Model of particle physics for very rare processes. In this context, weak decays of mesons and leptons play the prominent role besides the transitions between particles and antiparticles in which flavours of quarks and leptons are changed. In this manner, information about the Zeptouniverse corresponding to energy scales as high as 200 TeV or distances as small as 10^{-21} m can be obtained.

The year 1676 was very important for humanity, because Antoni van Leeuwenhoek discovered the empire of bacteria. He called these small creatures *animalcula* (small animals). His discovery was a milestone in our civilization for at least two reasons: He discovered creatures invisible to us which have been killing humans for thousands of years, often responsible for millions of deaths in one year. While Antoni van Leeuwenhoek did not know that bacteria could be dangerous for humans, his followers like Louis Pasteur, Robert Koch and other „microbe hunters" realized the danger coming from these tiny creatures and also developed weapons against this empire [1].

Van Leeuwenhoek was the first human who looked at short distance scales invisible to us and discovered thereby

No massive black holes in the Milky Way halo

Przemek Mróz[1*], Andrzej Udalski[1], Michał K. Szymański[1], Igor Soszyński[1], Łukasz Wyrzykowski[1], Paweł Pietrukowicz[1], Szymon Kozłowski[1], Radosław Poleski[1], Jan Skowron[1], Dorota Skowron[1], Krzysztof Ulaczyk[1,2], Mariusz Gromadzki[1], Krzysztof Rybicki[1,3], Patryk Iwanek[1], Marcin Wrona[1], Milena Ratajczak[1]

[1*]Astronomical Observatory, University of Warsaw, Al. Ujazdowskie 4, Warszawa, 00-478, Poland.
[2]Department of Physics, University of Warwick, Coventry CV4 7 AL, UK.
[3]Department of Particle Physics and Astrophysics, Weizmann Institute of Science, Rehovot 76100, Israel.

*Corresponding author(s). E-mail(s): pmroz@astrouw.edu.pl;

The gravitational wave detectors have unveiled a population of massive black holes that do not resemble those observed in the Milky Way [1–3]. They may have formed due to the evolution of massive low-metallicity stars [4], dynamical interactions in dense stellar environments [5, 6], or density fluctuations in the very early Universe (primordial black holes) [7–9]. If the latter hypothesis is correct, primordial black holes should comprise from several to 100% of dark matter to explain the black hole merger rates observed by gravitational wave detectors [10–12]. If such black holes existed in the Milky Way dark matter halo, they would cause long-timescale gravitational microlensing events lasting years. Here, we present the results of the search for the long-timescale microlensing events among the light curves of 78.7 million stars located in the Large Magellanic Cloud (LMC) that were monitored for 20 years (2001-2020) by the Optical Gravitational Lensing Experiment (OGLE) survey [13]. We did not find any events with timescales longer than one year. The properties of all thirteen microlensing events with timescales shorter than one year detected by OGLE toward the LMC can be explained by astrophysical objects located either in the LMC itself or in the Milky Way disk, without the need to invoke dark matter in the form of compact objects. We find that compact objects in the mass range from $1.8 \times 10^{-4}\,M_\odot$ to $6.3\,M_\odot$ cannot compose more than 1% of dark matter, and compact objects in the mass range from $1.3 \times 10^{-5}\,M_\odot$ to $860\,M_\odot$ cannot make up more than 10% of dark matter. This conclusively rules out primordial black hole mergers as a dominant source of gravitational waves.

Gravitational microlensing was proposed by [14] as a promising tool for searching for dark matter in the Milky Way halo. This idea prompted extensive searches by the first-generation microlensing surveys [15–18]. Here, we analyze the longest digital photometric data set to search for extremely long-timescale microlensing events. The data were collected for nearly 20 years during the third (OGLE-III; 2001–2009; [19]) and fourth (OGLE-IV; 2010–2020; [13]) phases of the OGLE project. Since OGLE-III and OGLE-IV had similar observing setups, it was possible to merge the observations to create a 20-year-long photometric time-series dataset. We developed a new method of reductions of photometric observations, which enabled us to obtain homogeneous light curves. The design of the survey, extraction of photometry, and methods used to search for microlensing events and calculate the event detection efficiency are described in detail in a companion paper [20].

About 33 million objects are detected in the overlapping OGLE-III/OGLE-IV region, and an additional 29 million objects are observed by OGLE-IV only. The number of stars that may be microlensed is even higher because of blending, which occurs when two or more stars cannot be resolved in ground-based seeing-limited images. We used the archival high-resolution images from the Hubble Space Telescope [21] to correct the star counts for blending. After removing the contribution from foreground Milky Way stars, we found that the survey monitored for microlensing about 78.7 million source stars in the LMC brighter than $I = 22$ mag [20].

We searched for microlensing events using a variation of the method described by [22]. The algorithm tries to identify a flat portion of the light curve, and then searches for consecutive data points that are magnified with respect to the flat part. Then, a standard point-source point-lens microlensing model [14] is fitted to the light curve, and the goodness-of-the-fit statistics are evaluated. The events are selected on the basis of a series of selection cuts. This procedure enabled us to find thirteen events that fulfill all detection criteria. Additionally, three events were identified by a manual inspection of the light curves, although they did not meet all selection criteria. The sample of thirteen events is used for a later statistical analysis [20].

We also carried out extensive light curve simulations to measure the event detection efficiency as a function of the event timescale [20]. To this end, we created synthetic light curves of microlensing events by injecting the microlensing signal into the light curves of constant stars observed by the project. Then, we measured the fraction of simulated events that passed all selection criteria. This procedure enabled us to take into account the noise in the data, as well as the effects of irregular sampling, gaps in the data, outliers, etc.

The contribution of primordial black holes (PBHs) and other compact objects to dark matter is often parameterized by $f = \Omega_{\rm PBH}/\Omega_{\rm DM}$, where $\Omega_{\rm PBH}$ is the density of dark matter in the form of PBHs and $\Omega_{\rm DM}$ is the density of dark matter. Note that we expect to detect some gravitational microlensing events even if $f = 0$: they come

Study of forbidden β decays within the realistic shell model

G. De Gregorio,[1,2] R. Mancino,[3,4,5] L. Coraggio,[1,2] and N. Itaco[1,2]

[1] *Dipartimento di Matematica e Fisica, Università degli Studi della Campania "Luigi Vanvitelli", viale Abramo Lincoln 5 - I-81100 Caserta, Italy*

[2] *Istituto Nazionale di Fisica Nucleare, Complesso Universitario di Monte S. Angelo, Via Cintia - I-80126 Napoli, Italy*

[3] *Institute of Particle and Nuclear Physics, Faculty of Mathematics and Physics, Charles University, V Holešovičkách 2, 180 00 Prague, Czech Republic*

[4] *Institut für Kernphysik (Theoriezentrum), Fachbereich Physik, Technische Universität Darmstadt, Schlossgartenstrasse 2 - 64298 Darmstadt, Germany*

[5] *GSI Helmholtzzentrum für Schwerionenforschung, Planckstrasse 1, 64291 Darmstadt, Germany*

For the first time, half-lives and energy spectra of forbidden β decays are calculated within the realistic shell model. Namely, we approach this issue starting from a realistic nucleon-nucleon potential and deriving effective Hamiltonians and decay operators. Our goal is to explore the sensitivity of the shape of calculated energy spectra to the renormalization of forbidden β-decay operators, an operation that allows to take into account those configurations that are not explicitly included in the chosen model space. The region that has been considered for this investigation are nuclei outside the ^{78}Ni core, more precisely we have studied the second-forbidden β decays of ^{94}Nb and ^{99}Tc, and fourth-forbidden β decays of ^{113}Cd and ^{115}In, that are currently of a renewed experimental interest in terms of novel spectroscopic techniques. Our results evidence that the introduction of a renormalized β-decay operator leads to a marked improvement of the reproduction of experimental half-lives. As regards the spectra of both second-forbidden and fourth-forbidden decays, we have found that their calculated shapes are in good agreement with the observed ones, even if scarcely responsive to the renormalization of the decay operator. We carry out also a detailed inspection of the different components of the calculated spectra for a deeper insight about their role in reproducing the experimental shapes.

PACS numbers: 21.60.Cs, 21.30.Fe, 27.60.+j

I. INTRODUCTION

The understanding of the renormalization mechanisms of electroweak currents is nowadays a cornerstone of the nuclear structure research. The attention to this issue is motivated by the need of calculating reliable nuclear matrix elements $M^{0\nu}$ for the $0\nu\beta\beta$ decay, and relating the inverse half-life $\left[T^{0\nu}_{1/2}\right]^{-1}$ of such a rare process to the neutrino effective mass.

As a matter of fact, the accurate calculation of the wave functions of parent and grand-daughter nuclei does not ensure a trustable $M^{0\nu}$, since most nuclear models are based on the reduction of the dimension of the Hilbert space where the nuclear Hamiltonian is defined. Then, a sound knowledge of the renormalization of the electroweak currents, to account for the configurations that are not explicitly included in the components of the nuclear wave function, is crucial to enhance the predictivity of the calculated $M^{0\nu}$s.

The ability of nuclear models to reproduce β-decay observables is, consequently, the better way to validate both wave functions and renormalization procedures, and such an issue is connected to the so-called "quenching puzzle" of the axial coupling constant, namely the need by most nuclear structure models to resort to a reduction of g_A to reproduce the observables directly linked to Gamow-Teller (GT) transitions [1–3]. However, this is an empirical procedure, and it cannot be generalized to any β-decay operator that depends on the value of the axial coupling constant.

The realistic shell model (RSM) provides a consistent approach to derive effective Hamiltonians and decay operators, the only parameter that is involved being the nuclear force one starts from. In such a framework, single-particle (SP) energies and two-body matrix elements (TBMEs) of the effective shell-model Hamiltonian $H_{\rm eff}$, as well as every matrix element of decay operators, are derived from a realistic free nucleon-nucleon (NN) potential V_{NN} by way of the many-body theory [4, 5]. The bare matrix elements of the NN potential, and of any transition operator, are renormalized with respect to the truncation of the full Hilbert space into the reduced shell-model (SM) model space, to take into account the neglected degrees of freedom without resorting to any empirical parameter [6]. In other words, this approach does not apply effective charges to calculate electromagnetic transition strengths, and empirical quenching of g_A to reproduce the β-decay matrix elements.

We have successfully employed RSM to study the $2\nu\beta\beta$-decay of ^{48}Ca, ^{76}Ge, ^{82}Se,^{100}Mo, ^{130}Te, and ^{136}Xe [7–10], and then extended it to predict the nuclear matrix elements of their $0\nu\beta\beta$-decay [9, 11]. Now, in order to validate the RSM in predicting β-decay observables, in the present work we investigate the sensitivity to the renormalization of SM forbidden β-decay operators describing the energy spectra of the emitted electrons.

To this end, we have considered the second-forbidden

Thomas K. Gaisser, a Pioneer of Particle Astrophysics

Francis Halzen[a], Paolo Lipari[b]

[a] *Department of Physics and*
Wisconsin IceCube Particle Astrophysics Center
UW–Madison, Madison, WI 53706 USA
[b] *INFN, Sezione Roma "Sapienza"*
Piazzale Aldo Moro 2, 00185 Roma, Italy

Abstract: We describe the pioneering contributions of Thomas K. Gaisser to the birth and development of particle astrophysics, a new field of research at the intersection of cosmic ray physics, astronomy, astrophysics, and particle physics that has emerged in the last few decades. We will especially focus on his studies of natural beams of neutrinos: those generated by the interactions of cosmic rays in the Earth's atmosphere and those emitted by astrophysical sources. Tom actively participated in the discovery of these cosmic neutrinos as well. His contributions also extend to gamma-ray astronomy, the study of the cosmic ray spectra and composition, and the modeling of cosmic ray interactions in the atmosphere and in astrophysical environments. Tom invariably focused his research on the theoretical and phenomenological problems of greatest interest at the time, producing frameworks that transparently interpreted often complex data. These studies have been very influential and have shaped the development of the field.

Starting in the late 1960s, the scientific life of Thomas K Gaisser spans more than five decades. This period saw the emergence and development of particle astrophysics, a new field of research at the intersection of cosmic ray physics, astronomy, astrophysics, and particle physics. If anyone could lay claim to the title of father of this new field of particle astrophysics, Tom could; he was also a true pioneer in gamma-ray and neutrino astronomy. His early career prepared him well, with research in particle and cosmic ray physics. He was a master of extracting science from the indirect information collected by air shower arrays, a skill he successfully applied in his later career to other particle astrophysics endeavors, most prominently the modeling of the atmospheric muon and neutrino fluxes. Tom's contributions to cosmic ray physics are reviewed in Ref. [1].

Early on, Tom studied the extensive air showers that are created when high-energy cosmic rays reach Earth. His contributions included the Gaisser-Hillas profile of longitudinal air showers developed in collaboration with Michael Hillas and the SIBYLL Monte Carlo for simulating air showers. He thus laid much of the groundwork for large experiments such as Auger and IceCube, and for how to use their data to probe fundamental questions in particle physics.

KEK preprint: 2023-55
Belle II preprint: 2024-007

Search for a $\mu^+\mu^-$ resonance in four-muon final states at Belle II

I. Adachi, K. Adamczyk, L. Aggarwal, H. Ahmed, H. Aihara, N. Akopov, A. Aloisio, N. Anh Ky, D. M. Asner, H. Atmacan, V. Aushev, M. Aversano, R. Ayad, V. Babu, H. Bae, S. Bahinipati, P. Bambade, Sw. Banerjee, S. Bansal, M. Barrett, J. Baudot, A. Baur, A. Beaubien, F. Becherer, J. Becker, J. V. Bennett, F. U. Bernlochner, V. Bertacchi, M. Bertemes, E. Bertholet, M. Bessner, S. Bettarini, B. Bhuyan, F. Bianchi, T. Bilka, S. Bilokin, D. Biswas, A. Bobrov, D. Bodrov, A. Bolz, A. Bozek, M. Bračko, P. Branchini, T. E. Browder, A. Budano, S. Bussino, M. Campajola, L. Cao, G. Casarosa, C. Cecchi, J. Cerasoli, M.-C. Chang, P. Chang, R. Cheaib, P. Cheema, B. G. Cheon, K. Chilikin, K. Chirapatpimol, H.-E. Cho, K. Cho, S.-J. Cho, S.-K. Choi, S. Choudhury, L. Corona, L. M. Cremaldi, S. Das, F. Dattola, E. De La Cruz-Burelo, S. A. De La Motte, G. De Nardo, M. De Nuccio, G. De Pietro, R. de Sangro, M. Destefanis, R. Dhamija, A. Di Canto, F. Di Capua, J. Dingfelder, Z. Doležal, T. V. Dong, M. Dorigo, K. Dort, S. Dreyer, S. Dubey, G. Dujany, P. Ecker, M. Eliachevitch, D. Epifanov, P. Feichtinger, T. Ferber, D. Ferlewicz, T. Fillinger, C. Finck, G. Finocchiaro, A. Fodor, F. Forti, A. Frey, B. G. Fulsom, A. Gabrielli, E. Ganiev, M. Garcia-Hernandez, R. Garg, G. Gaudino, V. Gaur, A. Gaz, A. Gellrich, G. Ghevondyan, D. Ghosh, H. Ghumaryan, G. Giakoustidis, R. Giordano, A. Giri, A. Glazov, B. Gobbo, R. Godang, O. Gogota, P. Goldenzweig, W. Gradl, T. Grammatico, E. Graziani, D. Greenwald, Z. Gruberová, T. Gu, K. Gudkova, S. Halder, Y. Han, T. Hara, H. Hayashii, S. Hazra, C. Hearty, M. T. Hedges, A. Heidelbach, I. Heredia de la Cruz, M. Hernández Villanueva, T. Higuchi, M. Hoek, M. Hohmann, P. Horak, C.-L. Hsu, T. Humair, T. Iijima, G. Inguglia, N. Ipsita, A. Ishikawa, R. Itoh, M. Iwasaki, P. Jackson, W. W. Jacobs, E.-J. Jang, Q. P. Ji, S. Jia, Y. Jin, K. K. Joo, H. Junkerkalefeld, D. Kalita, J. Kandra, K. H. Kang, G. Karyan, T. Kawasaki, F. Keil, C. Kiesling, C.-H. Kim, D. Y. Kim, K.-H. Kim, Y.-K. Kim, H. Kindo, K. Kinoshita, P. Kodyš, T. Koga, S. Kohani, K. Kojima, A. Korobov, S. Korpar, E. Kovalenko, R. Kowalewski, T. M. G. Kraetzschmar, P. Križan, P. Krokovny, T. Kuhr, J. Kumar, M. Kumar, R. Kumar, K. Kumara, T. Kunigo, A. Kuzmin, Y.-J. Kwon, S. Lacaprara, Y.-T. Lai, T. Lam, L. Lanceri, J. S. Lange, M. Laurenza, K. Lautenbach, R. Leboucher, F. R. Le Diberder, M. J. Lee, D. Levit, P. M. Lewis, C. Li, L. K. Li, Y. Li, Y. B. Li, J. Libby, M. Liu, Q. Y. Liu, Z. Q. Liu, D. Liventsev, S. Longo, T. Lueck, C. Lyu, Y. Ma, M. Maggiora, S. P. Maharana, R. Maiti, S. Maity, G. Mancinelli, R. Manfredi, E. Manoni, M. Mantovano, D. Marcantonio, S. Marcello, C. Marinas, L. Martel, C. Martellini, A. Martini, T. Martinov, L. Massaccesi, M. Masuda, K. Matsuoka, D. Matvienko, S. K. Maurya, J. A. McKenna, R. Mehta, F. Meier, M. Merola, F. Metzner, M. Milesi, C. Miller, M. Mirra, K. Miyabayashi, H. Miyake, R. Mizuk, G. B. Mohanty, N. Molina-Gonzalez, S. Mondal, S. Moneta, H.-G. Moser, M. Mrvar, R. Mussa, I. Nakamura, M. Nakao, Y. Nakazawa, A. Narimani Charan, M. Naruki, D. Narwal, Z. Natkaniec, A. Natochii, L. Nayak, M. Nayak, G. Nazaryan, C. Niebuhr, S. Nishida, S. Ogawa, Y. Onishchuk, H. Ono, Y. Onuki, P. Oskin, F. Otani, G. Pakhlova, A. Panta, S. Pardi, K. Parham, H. Park, S.-H. Park, B. Paschen, A. Passeri, S. Patra, S. Paul, T. K. Pedlar, R. Peschke, R. Pestotnik, M. Piccolo, L. E. Piilonen, G. Pinna Angioni, P. L. M. Podesta-Lerma, T. Podobnik, S. Pokharel, C. Praz, S. Prell, E. Prencipe, M. T. Prim, H. Purwar, P. Rados, G. Raeuber, S. Raiz, N. Rauls, M. Reif, S. Reiter, M. Remnev, I. Ripp-Baudot, G. Rizzo, S. H. Robertson, M. Roehrken, J. M. Roney, A. Rostomyan, N. Rout, G. Russo, D. A. Sanders, S. Sandilya, L. Santelj, Y. Sato, V. Savinov, B. Scavino, C. Schmitt, C. Schwanda, M. Schwickardi, Y. Seino, A. Selce, K. Senyo, J. Serrano, M. E. Sevior, C. Sfienti, W. Shan, C. P. Shen, X. D. Shi, T. Shillington, T. Shimasaki, J.-G. Shiu, D. Shtol, A. Sibidanov, F. Simon, J. B. Singh, J. Skorupa, R. J. Sobie, M. Sobotzik, A. Soffer, A. Sokolov, E. Solovieva, S. Spataro, B. Spruck, M. Starič, P. Stavroulakis, S. Stefkova, R. Stroili, M. Sumihama, K. Sumisawa, W. Sutcliffe, H. Svidras, M. Takizawa, U. Tamponi, S. Tanaka, K. Tanida, F. Tenchini, O. Tittel, R. Tiwary, D. Tonelli, E. Torassa, K. Trabelsi, I. Tsaklidis, M. Uchida, I. Ueda, K. Unger, Y. Unno, K. Uno, S. Uno,

P. Urquijo, Y. Ushiroda, S. E. Vahsen, R. van Tonder, K. E. Varvell, M. Veronesi, A. Vinokurova, V. S. Vismaya, L. Vitale, V. Vobbilisetti, R. Volpe, B. Wach, M. Wakai, S. Wallner, E. Wang, M.-Z. Wang, X. L. Wang, Z. Wang, A. Warburton, S. Watanuki, C. Wessel, E. Won, X. P. Xu, B. D. Yabsley, S. Yamada, W. Yan, S. B. Yang, J. Yelton, J. H. Yin, K. Yoshihara, C. Z. Yuan, Y. Yusa, L. Zani, B. Zhang, V. Zhilich, Q. D. Zhou, X. Y. Zhou, and V. I. Zhukova

(The Belle II Collaboration)

(Dated: March 5, 2024)

We report on a search for a resonance X decaying to a pair of muons in $e^+e^- \to \mu^+\mu^- X$ events in the 0.212–9.000 GeV/c^2 mass range, using 178 fb^{-1} of data collected by the Belle II experiment at the SuperKEKB collider at a center of mass energy of 10.58 GeV. The analysis probes two different models of X beyond the standard model: a Z' vector boson in the $L_\mu - L_\tau$ model and a muonphilic scalar. We observe no evidence for a signal and set exclusion limits at the 90% confidence level on the products of cross section and branching fraction for these processes, ranging from 0.046 fb to 0.97 fb for the $L_\mu - L_\tau$ model and from 0.055 fb to 1.3 fb for the muonphilic scalar model. For masses below 6 GeV/c^2, the corresponding constraints on the couplings of these processes to the standard model range from 0.0008 to 0.039 for the $L_\mu - L_\tau$ model and from 0.0018 to 0.040 for the muonphilic scalar model. These are the first constraints on the muonphilic scalar from a dedicated search.

PACS numbers:

I. INTRODUCTION

The standard model (SM) of particle physics is a highly predictive theoretical framework describing fundamental particles and their interactions. Despite its success, the SM is known to provide an incomplete description of nature. For example, it does not address the phenomenology related to dark matter, such as the observed relic density [1]. In addition, some experimental observations show inconsistencies with the SM. Prominent examples include the long-standing difference between the measured and the expected value of the muon anomalous magnetic-moment $(g-2)_\mu$ [2–4], possibly reduced by expectations based on lattice calculations [5], and the tensions in flavor observables reported by the BaBar, Belle, and LHCb experiments [6–8]. Some of these observations can be explained with the introduction of additional interactions, possibly lepton-universality-violating, mediated by non-SM neutral bosons [9–11]. Examples include the $L_\mu - L_\tau$ extension of the SM and a muonphilic scalar model.

The $L_\mu - L_\tau$ extension of the SM [12–14] gauges the difference between the muon and the τ-lepton numbers, giving rise to a new massive, neutral vector boson, the Z'. Among the SM particles, this particle couples only to μ, τ, ν_μ, and ν_τ, with a coupling constant g'. The Z' could also mediate interactions between SM and dark matter.

The muonphilic scalar S is primarily proposed as a solution for the $(g-2)_\mu$ anomaly [15–18]. This particle couples exclusively to muons through a Yukawa-like interaction, which is not gauge-invariant under the SM gauge symmetry and may arise from a high-dimension operator term at a mass scale beyond the SM. In contrast to the $L_\mu - L_\tau$ model, the muonphilic scalar model needs a high-energy completion.

Searches for a Z' decaying to muons have been reported by the BaBar [19], Belle [20], and CMS [21] Collaborations. An invisibly decaying Z' has been searched for by the Belle II [22, 23] and NA64-e [24] experiments. The Belle II experiment also searched recently for a Z' decaying to $\tau^+\tau^-$ [25]. Constraints on the existence of a muonphilic scalar have been obtained by reinterpretations of Z' searches into muons [18]. However, important experimental details may be unaccounted for in these reinterpretation studies, including the significantly different kinematic properties of the signal and the corresponding variation of the efficiency.

Here we report a search for the process $e^+e^- \to \mu^+\mu^- X$, with $X \to \mu^+\mu^-$, where X indicates Z' or S. The signal signature is a narrow enhancement in the mass distribution of oppositely charged muons $M(\mu\mu)$ in $e^+e^- \to \mu^+\mu^-\mu^+\mu^-$ events. We use data collected by the Belle II experiment at a center-of-mass (c.m.) energy $\sqrt{s}$ corresponding to the mass of the $\Upsilon(4S)$ resonance. The $L_\mu - L_\tau$ model is used as a benchmark to develop the analysis; we then apply the same selections to the muonphilic scalar model and evaluate the performance. In both models, the X particle is at leading order emitted as final-state radiation (FSR) from one of the muons, as shown in Fig. 1. For the range of couplings explored in this study, the lifetime of X is negligible compared to the experimental resolution. The analysis techniques are optimized using simulated events prior to examining data.

We select events with exactly four charged particles with zero net charge, where at least three are identified as muons, with an invariant mass $M(4\mu)$ close to $\sqrt{s}/c^2$, and with negligible extra energy in the event. The dominant, non-peaking background is the SM $e^+e^- \to \mu^+\mu^-\mu^+\mu^-$ process, whose main production diagrams are shown in Fig. 2. The analysis uses kinematic variables combined with a multivariate technique to enhance the signal-to-background ratio. A kinematic fit improves the dimuon mass resolution. The signal yield is extracted through a

EUROPEAN ORGANISATION FOR NUCLEAR RESEARCH (CERN)

Submitted to: EPJC

CERN-EP-2024-048
6th March 2024

Fiducial and differential cross-section measurements of electroweak $W\gamma jj$ production in pp collisions at $\sqrt{s}$ = 13 TeV with the ATLAS detector

The ATLAS Collaboration

The observation of the electroweak production of a W boson and a photon in association with two jets, using pp collision data at the Large Hadron Collider at a centre of mass energy of $\sqrt{s}$ = 13 TeV, is reported. The data were recorded by the ATLAS experiment from 2015 to 2018 and correspond to an integrated luminosity of 140 fb^{-1}. This process is sensitive to the quartic gauge boson couplings via the vector boson scattering mechanism and provides a stringent test of the electroweak gauge symmetry breaking of the Standard Model. Events are selected if they contain one electron or muon, missing transverse momentum, at least one photon, and two jets. Multivariate techniques are used to distinguish the electroweak $W\gamma jj$ process from irreducible background processes. The observed significance of the electroweak $W\gamma jj$ process is well above six standard deviations, compared to an expected significance of 6.3 standard deviations. Fiducial and differential cross sections are measured in a fiducial phase space close to the detector acceptance, which are in reasonable agreement with leading order Standard Model predictions from MadGraph5+Pythia8 and Sherpa. The results are used to constrain new physics effects in the context of an effective field theory.

Contents

1 Introduction

The scattering of two vector bosons, e.g. $WZ \to W\gamma$, is sensitive to both the triple and quartic electroweak-boson self-interactions [1, 2]. Consequently, vector boson scattering (VBS) provides an excellent opportunity to probe the nature of the electroweak (EW) gauge symmetry breaking of the Standard Model (SM).

In proton–proton (pp) collisions, the $W\gamma jj$ final state can be produced via many different mechanisms, as shown in Figure 1. Electroweak $W\gamma jj$ production concerns exclusively electroweak interactions of order α_{EW}^4 at tree level [3], where α_{EW} is the electroweak coupling constant. Although the contributions of interest are VBS interactions involving quartic gauge couplings (QGCs), these cannot be distinguished from other electroweak contributions in a gauge-invariant manner. Thus, the signal process studied in this paper is the combination of all processes of order α_{EW}^4 shown in Figures 1(a)-1(c). The dominant background for EW $W\gamma jj$ production concerns processes of order $\alpha_{\mathrm{S}}^2\alpha_{\mathrm{EW}}^2$ at tree level in Figure 1(d), where α_{S} is the strong coupling constant and the jets are produced via strong interaction vertices; these processes are collectively referred to as strong $W\gamma jj$ production in this paper. Triboson diagrams, such as the one shown in Figure 1(b), do contribute to EW $W\gamma jj$ production. However, due to their distinct topology they require separate signal selection and background estimation methods and are thus generally the subject of separate studies.

EUROPEAN ORGANISATION FOR NUCLEAR RESEARCH (CERN)

Submitted to: JHEP

CERN-EP-2024-034
6th March 2024

Differential cross-sections for events with missing transverse momentum and jets measured with the ATLAS detector in 13 TeV proton–proton collisions

The ATLAS Collaboration

Measurements of inclusive, differential cross-sections for the production of events with missing transverse momentum in association with jets in proton–proton collisions at $\sqrt{s}$ = 13 TeV are presented. The measurements are made with the ATLAS detector using an integrated luminosity of 140 fb^{-1} and include measurements of dijet distributions in a region in which vector-boson fusion processes are enhanced. They are unfolded to correct for detector resolution and efficiency within the fiducial acceptance, and are designed to allow robust comparisons with a wide range of theoretical predictions. A measurement of differential cross sections for the $Z \to \nu\nu$ process is made. The measurements are generally well-described by Standard Model predictions except for the dijet invariant mass distribution. Auxiliary measurements of the hadronic system recoiling against isolated leptons, and photons, are also made in the same phase space. Ratios between the measured distributions are then derived, to take advantage of cancellations in modelling effects and some of the major systematic uncertainties. These measurements are sensitive to new phenomena, and provide a mechanism to easily set constraints on phenomenological models. To illustrate the robustness of the approach, these ratios are compared with two common Dark Matter models, where the constraints derived from the measurement are comparable to those set by dedicated detector-level searches.

Contents

Real-time portable muography with Hankuk Atmospheric-muon Wide Landscaping : HAWL

J. Seo[a], N. Carlin[b], D. F. F. S. Cavalcante[b], J. S. Chung[a], L. E. França[b], C. Ha[a,1], J. Kim[a], J. Y. Kim[a], H. Kimku[a], B. C. Koh[a], Y. J. Lee[a], B. B. Manzato[b], S. W. Oh[a], R. L. C. Pitta[b], S. J. Won[a]

[a]*Department of Physics, Chung-Ang University, Seoul, 06974, Republic of Korea*
[b]*Physics Institute, University of São Paulo, São Paulo, 05508-090, Brazil*

Abstract

Cosmic ray muons prove valuable across various fields, from particle physics experiments to non-invasive tomography, thanks to their high flux and exceptional penetrating capability. Utilizing a scintillator detector, one can effectively study the topography of mountains situated above tunnels and underground spaces. The Hankuk Atmospheric-muon Wide Landscaping (HAWL) project successfully charts the mountainous region of eastern Korea by measuring cosmic ray muons with a detector in motion. The real-time muon flux measurement shows a tunnel length accuracy of 6.5 %, with a detectable overburden range spanning from 8 to 400 meter-water-equivalent depth. This is the first real-time portable muon tomography.

Keywords: Muon tomography, Plastic scintillator, Portable radiation detector

1. Introduction

A cosmic-ray muon is an elementary particle generated when a primary cosmic-ray particle collides with atmospheric nuclei Workman et al. (2022). Cosmic-ray muons, in abundance, can traverse high-density materials non-destructively, and their unique energy loss in a material renders them valuable in various applications, from particle physics experiments to muon tomography. In particle physics experiments, a high spatial and temporal resolution muon counter can measure muon flux, track final state particles in an accelerator beam Hewes et al. (2021), and reveal yearly modulations with zenith angle dependence Tilav et al. (2020). Muon tomography has uncovered unknown spaces within pyramids Procureur et al. (2023b) and is employed to assess the condition of nuclear power plants Procureur et al. (2023a). Furthermore, recent advancements in high-resolution muon imaging technology and portable detectors have broadened their applications, notably in volcanic activity detection Tioukov et al. (2019) and archaeological site investigations Avgitas et al. (2022).

The primary goal of this research is to map the land forms and features above the underground spaces quickly and non-invasively using a moving muon detector. To reconstruct mountainous topography using measured muon flux, we launched the Hankuk Atmospheric-muon Wide Landscaping (HAWL) project. HAWL precisely gauges changes in muon flux within tunnels situated above the Seoul-Yangyang highway and Yangyang Underground Laboratory (Y2L) Adhikari et al. (2018a) in South Korea while moving in high speed as schematically shown in Fig. 1. With data collected by the HAWL detector, we measured the muon flux as a function of elevation, and the detector sensitivity in terms of depth and length resolutions for the tunnels.

Email address: chha@cau.ac.kr (C. Ha)

Measurement of CP asymmetries in $B^0 \to K^0_S K^0_S K^0_S$ decays at Belle II

I. Adachi, L. Aggarwal, H. Ahmed, H. Aihara, N. Akopov, A. Aloisio, N. Anh Ky, D. M. Asner, H. Atmacan, T. Aushev, V. Aushev, M. Aversano, R. Ayad, V. Babu, H. Bae, S. Bahinipati, P. Bambade, Sw. Banerjee, S. Bansal, M. Barrett, J. Baudot, M. Bauer, A. Baur, A. Beaubien, F. Becherer, J. Becker, P. K. Behera, J. V. Bennett, F. U. Bernlochner, V. Bertacchi, M. Bertemes, E. Bertholet, M. Bessner, S. Bettarini, B. Bhuyan, F. Bianchi, L. Bierwirth, T. Bilka, D. Biswas, A. Bobrov, D. Bodrov, A. Bolz, A. Bondar, J. Borah, A. Bozek, M. Bračko, P. Branchini, R. A. Briere, T. E. Browder, A. Budano, S. Bussino, M. Campajola, L. Cao, G. Casarosa, C. Cecchi, J. Cerasoli, M.-C. Chang, P. Chang, R. Cheaib, P. Cheema, V. Chekelian, C. Chen, B. G. Cheon, K. Chilikin, K. Chirapatpimol, H.-E. Cho, K. Cho, S.-J. Cho, S.-K. Choi, S. Choudhury, J. Cochran, L. Corona, L. M. Cremaldi, S. Das, F. Dattola, E. De La Cruz-Burelo, S. A. De La Motte, G. De Nardo, M. De Nuccio, G. De Pietro, R. de Sangro, M. Destefanis, S. Dey, A. De Yta-Hernandez, R. Dhamija, A. Di Canto, F. Di Capua, J. Dingfelder, Z. Doležal, I. Domínguez Jiménez, T. V. Dong, M. Dorigo, K. Dort, D. Dossett, S. Dreyer, S. Dubey, G. Dujany, P. Ecker, M. Eliachevitch, D. Epifanov, P. Feichtinger, T. Ferber, D. Ferlewicz, T. Fillinger, C. Finck, G. Finocchiaro, A. Fodor, F. Forti, A. Frey, B. G. Fulsom, A. Gabrielli, E. Ganiev, M. Garcia-Hernandez, R. Garg, A. Garmash, G. Gaudino, V. Gaur, A. Gaz, A. Gellrich, G. Ghevondyan, D. Ghosh, H. Ghumaryan, G. Giakoustidis, R. Giordano, A. Giri, A. Glazov, B. Gobbo, R. Godang, O. Gogota, P. Goldenzweig, W. Gradl, T. Grammatico, S. Granderath, E. Graziani, D. Greenwald, Z. Gruberová, T. Gu, Y. Guan, K. Gudkova, S. Halder, Y. Han, K. Hara, T. Hara, K. Hayasaka, H. Hayashii, S. Hazra, C. Hearty, M. T. Hedges, A. Heidelbach, I. Heredia de la Cruz, M. Hernández Villanueva, A. Hershenhorn, T. Higuchi, E. C. Hill, M. Hoek, M. Hohmann, P. Horak, C.-L. Hsu, T. Humair, T. Iijima, K. Inami, N. Ipsita, A. Ishikawa, S. Ito, R. Itoh, M. Iwasaki, P. Jackson, W. W. Jacobs, D. E. Jaffe, E.-J. Jang, Q. P. Ji, S. Jia, Y. Jin, A. Johnson, K. K. Joo, H. Junkerkalefeld, H. Kakuno, M. Kaleta, D. Kalita, A. B. Kaliyar, J. Kandra, K. H. Kang, S. Kang, G. Karyan, T. Kawasaki, F. Keil, C. Ketter, C. Kiesling, C.-H. Kim, D. Y. Kim, K.-H. Kim, Y.-K. Kim, H. Kindo, K. Kinoshita, P. Kodyš, T. Koga, S. Kohani, K. Kojima, T. Konno, A. Korobov, S. Korpar, E. Kovalenko, R. Kowalewski, T. M. G. Kraetzschmar, P. Križan, P. Krokovny, Y. Kulii, T. Kuhr, J. Kumar, M. Kumar, R. Kumar, K. Kumara, T. Kunigo, A. Kuzmin, Y.-J. Kwon, S. Lacaprara, Y.-T. Lai, T. Lam, L. Lanceri, J. S. Lange, M. Laurenza, K. Lautenbach, R. Leboucher, F. R. Le Diberder, P. Leitl, D. Levit, C. Li, L. K. Li, Y. Li, J. Libby, Q. Y. Liu, Z. Q. Liu, D. Liventsev, S. Longo, A. Lozar, T. Lueck, C. Lyu, Y. Ma, M. Maggiora, S. P. Maharana, R. Maiti, S. Maity, G. Mancinelli, R. Manfredi, E. Manoni, M. Mantovano, D. Marcantonio, S. Marcello, C. Marinas, L. Martel, C. Martellini, A. Martini, T. Martinov, L. Massaccesi, M. Masuda, T. Matsuda, D. Matvienko, S. K. Maurya, J. A. McKenna, R. Mehta, F. Meier, M. Merola, F. Metzner, M. Milesi, C. Miller, M. Mirra, K. Miyabayashi, H. Miyake, R. Mizuk, G. B. Mohanty, N. Molina-Gonzalez, S. Mondal, S. Moneta, H.-G. Moser, M. Mrvar, R. Mussa, I. Nakamura, K. R. Nakamura, M. Nakao, Y. Nakazawa, A. Narimani Charan, M. Naruki, Z. Natkaniec, A. Natochii, L. Nayak, M. Nayak, G. Nazaryan, M. Neu, C. Niebuhr, N. K. Nisar, S. Nishida, S. Ogawa, Y. Onishchuk, H. Ono, Y. Onuki, P. Oskin, F. Otani, P. Pakhlov, G. Pakhlova, A. Paladino, A. Panta, E. Paoloni, S. Pardi, K. Parham, H. Park, S.-H. Park, B. Paschen, A. Passeri, S. Patra, S. Paul, T. K. Pedlar, I. Peruzzi, R. Peschke, R. Pestotnik, F. Pham, M. Piccolo, L. E. Piilonen, G. Pinna Angioni, P. L. M. Podesta-Lerma, T. Podobnik, S. Pokharel, C. Praz, S. Prell, E. Prencipe, M. T. Prim, H. Purwar, N. Rad, P. Rados, G. Raeuber, S. Raiz, N. Rauls, M. Reif, S. Reiter, M. Remnev, I. Ripp-Baudot, G. Rizzo, L. B. Rizzuto, S. H. Robertson, M. Roehrken, J. M. Roney, A. Rostomyan, N. Rout, G. Russo, D. Sahoo, D. A. Sanders, S. Sandilya, A. Sangal, L. Santelj, Y. Sato, V. Savinov, B. Scavino, C. Schmitt, C. Schwanda, A. J. Schwartz, Y. Seino, A. Selce, K. Senyo, J. Serrano, M. E. Sevior, C. Sfienti, W. Shan, C. Sharma, X. D. Shi, T. Shillington, T. Shimasaki, J.-G. Shiu, D. Shtol, B. Shwartz, A. Sibidanov, F. Simon, J. B. Singh, J. Skorupa, R. J. Sobie, M. Sobotzik, A. Soffer, A. Sokolov, E. Solovieva, S. Spataro, B. Spruck, M. Starič, P. Stavroulakis, S. Stefkova, Z. S. Stottler, R. Stroili, J. Strube, Y. Sue, M. Sumihama, K. Sumisawa, W. Sutcliffe, H. Svidras, M. Takahashi, M. Takizawa, U. Tamponi, K. Tanida, H. Tanigawa, F. Tenchini,

A. Thaller, O. Tittel, R. Tiwary, D. Tonelli, E. Torassa, N. Toutounji, K. Trabelsi, I. Tsaklidis, M. Uchida, I. Ueda, Y. Uematsu, T. Uglov, K. Unger, Y. Unno, K. Uno, S. Uno, P. Urquijo, Y. Ushiroda, S. E. Vahsen, R. van Tonder, G. S. Varner, K. E. Varvell, M. Veronesi, V. S. Vismaya, L. Vitale, V. Vobbilisetti, R. Volpe, B. Wach, M. Wakai, S. Wallner, E. Wang, M.-Z. Wang, X. L. Wang, Z. Wang, A. Warburton, M. Watanabe, S. Watanuki, M. Welsch, C. Wessel, X. P. Xu, B. D. Yabsley, S. Yamada, W. Yan, S. B. Yang, J. Yelton, J. H. Yin, K. Yoshihara, C. Z. Yuan, Y. Yusa, L. Zani, Y. Zhang, V. Zhilich, J. S. Zhou, Q. D. Zhou, X. Y. Zhou, and V. I. Zhukova

(The Belle II Collaboration)

We report a measurement of decay-time dependent charge-parity (CP) asymmetries in $B^0 \to K^0_S K^0_S K^0_S$ decays. We use 387×10^6 $B\overline{B}$ pairs collected at the $\Upsilon(4S)$ resonance with the Belle II detector at the SuperKEKB asymmetric-energy electron-positron collider. We reconstruct 220 signal events and extract the CP-violating parameters S and C from a fit to the distribution of the decay-time difference between the two B mesons. The resulting confidence region is consistent with previous measurements in $B^0 \to K^0_S K^0_S K^0_S$ and $B^0 \to (c\bar{c})K^0$ decays, and with predictions based on the standard model.

I. INTRODUCTION

In the standard model (SM), the charmless three-body decay $B^0 \to K^0_S K^0_S K^0_S$ is mediated by the $b \to sq\bar{q}$ quark transition, which is dominated by a one-loop process, the so-called penguin amplitude. Charge-conjugate decays are implied hereafter unless specified otherwise. Penguin amplitudes are suppressed in the SM, e.g, $\mathcal{B}(B^0 \to K^0_S K^0_S K^0_S) = (6.0 \pm 0.5) \times 10^{-6}$ [1], and imply exchanges of virtual particles where SM particles can be replaced by a broad class of non-SM particles. These features make these decays sensitive to possible contributions from non-SM physics [2]. A key probe of such contributions is provided by decay-time dependent CP-violating asymmetries of the B^0 and $\overline{B}^0$ decay rates. These asymmetries arise from interference between amplitudes for direct decay and decay following flavor oscillations, due to the irreducible phase in the Cabibbo-Kobayashi-Maskawa (CKM) quark-mixing matrix [3]. Precise measurements of these asymmetries using $B^0\overline{B}^0$ pairs are a primary goal of experiments in electron-positron collisions at the $\Upsilon(4S)$ resonance. If one of the neutral B mesons, B_{CP}, decays into a CP eigenstate f_{CP} at proper time t_{CP} and the other, $B_{\rm tag}$, decays into a flavor-specific final state $f_{\rm tag}$ at proper time $t_{\rm tag}$, the probability density for observing a $B_{\rm tag}$ with flavor q_f at $\Delta t \equiv t_{CP} - t_{\rm tag}$ is [4–6]

$$\mathcal{P}(\Delta t, q_f) = \frac{e^{-|\Delta t|/\tau_{B^0}}}{4\tau_{B^0}} \Big(1 + q_f \big[S \sin(\Delta m_d \Delta t) - C \cos(\Delta m_d \Delta t) \big] \Big), \quad (1)$$

where the flavor q_f is $+1(-1)$ for $B_{\rm tag} = B^0(\overline{B}^0)$, τ_{B^0} is the B^0 lifetime, Δm_d is the mass difference between the two mass eigenstates of the B^0-$\overline{B}^0$ system, and the CP asymmetries S and C express mixing-induced and direct CP violation, respectively[7]. The SM predicts that $S = -\sin 2\phi_1 - 0.02$ and $C = -0.007$ for decays into the CP-even final state $K^0_S K^0_S K^0_S$ [8]. The mixing phase $\phi_1 \equiv \arg[-V_{cd}V^*_{cb}/V_{td}V^*_{tb}]$ is a combination of CKM matrix-elements. The uncertainty in the SM prediction for S is smaller than 0.01; hence, a large deviation in $B^0 \to K^0_S K^0_S K^0_S$ decays would indicate non-SM physics. The Belle [9] and BaBar [10] experiments reported these asymmetries with comparable uncertainties dominated by the sample size, yielding world-average values $S = -0.83 \pm 0.17$ and $C = -0.15 \pm 0.12$ [11]. While these agree with the SM predictions, the large uncertainties limit the sensitivity to non-SM sources. Additional measurements are needed.

We report a measurement of S and C in $B^0 \to K^0_S K^0_S K^0_S$ decays using electron-positron collisions at the $\Upsilon(4S)$ collected by the Belle II experiment. We reconstruct signal (B_{CP}) $B^0 \to K^0_S K^0_S K^0_S$ decays followed by $K^0_S \to \pi^+\pi^-$ decays and suppress background using two multivariate classifiers. We then measure q_f using the remaining charged particles in the event and Δt from the distance between the decay positions of B_{CP} and $B_{\rm tag}$. We divide the $B^0 \to K^0_S K^0_S K^0_S$ events into two classes based on the quality of the Δt information: time-differential (TD) events use Δt and determine S and C, while time-integrated (TI) events do not use Δt and contribute to the determination of C only. Fits to signal-discriminating observables and decay time (when appropriate) determine the signal yield and CP asymmetries. We use the decay $B^+ \to K^0_S K^0_S K^+$ as a control channel to constrain the fit model from data.

II. THE BELLE II DETECTOR AND DATA SAMPLE

The Belle II experiment is located at SuperKEKB, which collides electrons and positrons at and near the $\Upsilon(4S)$ resonance [12]. The Belle II detector [13] has a cylindrical geometry and includes a six-layer silicon detector (VXD) and a 56-layer central drift chamber (CDC). These detectors reconstruct trajectories of charged particles (tracks). The VXD consists of two layers of silicon-pixel detectors (PXD) surrounded by four layers of double-sided silicon-strip detectors [14]. Only

Two-particle angular correlations of identified particles in pp and p–Pb collisions at LHC energies with ALICE

Daniela Ruggiano

Warsaw University of Technology – Warsaw, Poland

Summary. — The two-particle angular correlations in the Δy,$\Delta\varphi$ space provide valuable insights into the properties of hadronization mechanisms and quark–gluon plasma properties. The correlation functions are influenced by several physical sources, including mini-jet correlations, Bose–Einstein quantum statistics, resonance decays, conservation of energy and momentum, and other factors. Each correlation source has unique properties, and therefore each correlation function has a distinct form depending on transverse momentum and/or multiplicity. Previous results from angular correlation analysis of pp collisions at the LHC energies indicate an anti-correlation for pairs of baryons of the same sign in $\Delta\eta, \Delta\varphi$ space. This contradicts the predictions of Monte Carlo models, such as PYTHIA8 and EPOS.
This study aims to investigate this behavior by exploring the correlation functions of different charge combinations of the detected particles (specifically, $\pi^{\pm}$, $K^{\pm}$, and $p\bar{p}$) and multiplicity classes in the $\Delta y, \Delta\varphi$ space for pp and p–Pb collisions at LHC energies. In addition, the study includes a comparison of the results obtained from both collision systems.

1. – Introduction

The lack of a clear understanding of the production processes of one of the most abundant and fundamental particles in the universe, the proton, is one of the open and unresolved questions in the field of nuclear physics. Angular correlations are a powerful tool used to describe the mechanism of particle production in high-energy heavy-ion collisions. They are influenced by multiple effects such as (mini)jets, Bose–Einstein or Fermi–Dirac quantum statistics (in the case of identical bosons or fermions), resonance decays, Coulomb interactions, conservation of energy and momentum, and others, all of which contribute with some structure to the overall shape. Moreover, each correlation shows a unique behavior with its shape, and its individuality, as already observed in studies of proton–proton (pp) collisions at $\sqrt{s} = 7$ TeV by the ALICE Collaboration at LHC [1]. In particular, correlations of baryon–baryon pairs (combined with antibaryon–

EUROPEAN ORGANISATION FOR NUCLEAR RESEARCH (CERN)

Submitted to: Physics Reports

CERN-EP-2024-056
6th March 2024

The quest to discover supersymmetry at the ATLAS experiment

The ATLAS Collaboration

The search for supersymmetry with the ATLAS experiment at the CERN Large Hadron Collider intensified after the discovery of the Higgs boson in 2012. The search programme expanded in both breadth and depth, profiting from the increased integrated luminosity and higher centre-of-mass energy of Run 2, and gaining new sensitivity to unexplored areas of supersymmetry parameter space through the use of new experimental signatures and innovative analysis techniques. This report summarises the supersymmetry searches at ATLAS using up to 140 fb^{-1} of pp collisions at $\sqrt{s} = 13$ TeV, including the limits set on the production of gluinos, squarks, and electroweakinos for scenarios either with or without R-parity conservation, and including models where some of the supersymmetric particles are long-lived.

Contents

1 Introduction

One of the most significant contributions of the CERN Large Hadron Collider (LHC) [1] to high-energy physics comes through the particles that the ATLAS [2] and CMS [3] collaborations have *not* found. Both collaborations have pursued an unprecedented programme of searches for phenomena not predicted by the Standard Model (SM). The wide variety of signatures explored, and the richness of the models considered, has had a powerful influence on community's paradigms of physics beyond the Standard Model.

Among these paradigms, supersymmetry (SUSY) [4–9] is one of the most closely examined. The approach of imposing symmetries on Lagrangians led to the construction of electroweak theory, the unification of the weak and electromagnetic interaction and, eventually, the development of the Standard Model. The phenomenology of SUSY stems from requiring the Lagrangian to be invariant under an operator that maps fermionic fields into bosonic ones, and vice versa. It was found that only additional space-time symmetry could be added to the Poincaré group [5]. To impose this symmetry, one needs to add many new *superpartners* of the Standard Model particles. The much richer particle content, and some of the free parameters that one needs to add to make SUSY a broken symmetry (for example, it is known that there is no superpartner of the electron with mass $m = 0.511$ MeV), makes SUSY an ideal framework to accommodate many of the shortcomings of the Standard Model. The quantum corrections to the Higgs boson mass coming from the fermions are counterbalanced by those coming from their superpartners, stabilising the mass to a value near the electroweak scale in a natural way. On top of that, the modified particle content changes the evolution of the running gauge couplings of the SM, potentially allowing

ACE Science Workshop Report

Stefania Gori (ed.)[1], Nhan Tran (ed.)[2], Karri DiPetrillo[3], Bertrand Echenard[4], Jeffrey Eldred[2], Roni Harnik[2], Pedro Machado[2], Matthew Toups[2], I. P. Fernando[5], Robert Bernstein[2], Innes Bigaran[2,6], Cari Cesarotti[9], Bhaskar Dutta[7], Christian Herwig[2], Sergo Jindariani[2], Ryan Plestid[4], Vladimir Shiltsev[10], Matthew Solt[5], Alexandre Sousa[8], Diktys Stratakis[2], Zahra Tabrizi[6], Anil Thapa[5], Jacob Zettlemoyer[2], and Jure Zupan[8]

[1]University of California Santa Cruz, Santa Cruz, CA 95064, USA
[2]Fermi National Accelerator Laboratory, Batavia, IL 60510, USA
[3]University of Chicago, Chicago, IL 60637, USA
[4]California Institute of Technology, Pasadena, CA 91125, USA
[5]University of Virginia, Charlottesville, VA 22904, USA
[6]Northwestern University, Evanston, IL 60208, USA
[7]Mitchell Institute and Texas A&M University, College Station, TX 77843, USA
[8]University of Cincinnati, Cincinnati, OH 45221, USA
[9]Massachusetts Institute of Technology, Cambridge, MA 02139, USA
[10]Northern Illinois University, DeKalb, IL 60115, USA

ABSTRACT

We summarize the Fermilab Accelerator Complex Evolution (ACE) Science Workshop, held on June 14-15, 2023. The workshop presented the strategy for the ACE program in two phases: ACE Main Injector Ramp and Target (MIRT) upgrade and ACE Booster Replacement (BR) upgrade. Four plenary sessions covered the primary experimental physics thrusts: Muon Collider, Neutrinos, Charged Lepton Flavor Violation, and Dark Sectors. Additional physics and technology ideas were presented from the community that could expand or augment the ACE science program. Given the physics framing, a parallel session at the workshop was dedicated to discussing priorities for accelerator R&D. Finally, physics discussion sessions concluded the workshop where experts from the different experimental physics thrusts were brought together to begin understanding the synergies between the different physics drivers and technologies. In December of 2023, the P5 report was released setting the physics priorities for the field in the next decade and beyond, and identified ACE as an important component of the future US accelerator-based program. Given the presentations and discussions at the ACE Science Workshop and the findings of the P5 report, we lay out the topics for study to determine the physics priorities and design goals of the Fermilab ACE project in the near-term.

Translationally invariant shell model calculation of the quasielastic $(p, 2p)$ process at intermediate relativistic energies

A.B. Larionov[1a], Yu.N. Uzikov[2,3,4b]

[1] *Bogoliubov Laboratory of Theoretical Physics, Joint Institute for Nuclear Research, 141980 Dubna, Russia*

[2] *Laboratory of Nuclear Problems, Joint Institute for Nuclear Research, 141980 Dubna, Russia*

[3] *Department of Physics, Moscow State University, 119991 Moscow, Russia*

[4] *Dubna State University, 141980 Dubna, Russia*

Abstract

Relativistic beams of heavy ions interacting with various nuclear targets allow to study a broad range of problems starting from nuclear equation of state to the traditional nuclear structure. Some questions which were impossible to answer heretofore – can be addressed nowadays by using inverse kinematics. These includes the structure of short-lived nuclei and the precision study of exclusive channels with production of residual nuclei in certain quantum states. Theoretical understanding such processes is so far based on factorization models which combine the single-step amplitude of the reaction on a bound nucleon or nuclear cluster with a certain wave function of its relative motion with respect to the residual nucleus. The nuclear structure information is encoded in the spectroscopic amplitude, calculable within nuclear many-body theories. In this work, we use for this purpose the translationally-invariant shell model with configuration mixing and demonstrate that it successfully reproduces the single-differential and integrated cross sections of the quasielastic proton knockout, ^{12}C$(p, 2p)^{11}$B, with outgoing ^{11}B in the ground state and low-lying excited states measured at GSI at 400 MeV/nucleon.

[a] e-mail: larionov@theor.jinr.ru

[b] e-mail: uzikov@jinr.ru

What Can We Learn from Directed Flow at STAR-FTX Energies?

Yu. B. Ivanov[1, 2, *] and M. Kozhevnikova[3, †]

[1] *Bogoliubov Laboratory of Theoretical Physics, JINR Dubna, 141980 Dubna, Russia*
[2] *National Research Center "Kurchatov Institute", 123182 Moscow, Russia*
[3] *Veksler and Baldin Laboratory of High Energy Physics, JINR Dubna, 141980 Dubna, Russia*

We present results of simulations of directed flow of various hadrons in Au+Au collisions at collision energies of $\sqrt{s_{NN}} = 3$ and 4.5 GeV. Simulations are performed within the model three-fluid dynamics (3FD) and the event simulator based on it (THESEUS). The results are compared with recent STAR data. The directed flows of various particles provide information on dynamics in various parts and at various stages of the colliding system depending on the particle. However, the information on the equation of state is not always directly accessible because of strong influence of the afterburner stage or insufficient equilibration of the matter. It is found that the crossover scenario gives the best overall description of the data. This crossover EoS is soft in the hadronic phase. The transition into QGP in Au+Au collisions occurs at collision energies between 3 and 4.5 GeV, at baryon densities $n_B \gtrsim 4n_0$ and temperatures ≈ 150 MeV. In-medium effects in the directed flow of (anti)kaons are discussed.

I. INTRODUCTION

The directed flow is one of the most sensitive quantities to the dynamics of nucleus-nucleus collisions and properties of the matter produced in these collisions. It provides information about the stopping power of the nuclear matter, its equation of state (EoS), transition to quark-gluon phase (QGP) and more. All these issues were addressed in the analysis of the STAR data [1] obtained within Beam Energy Scan (BES) program at the Relativistic Heavy-Ion Collider (RHIC). The analysis was performed within various approaches [2–14], which include both hydrodynamic and kinetic models. An important conclusion of these studies is that the transition to the quark-gluon phase is most probably of the crossover or weak-first-order type and it stars at collision energies of $\sqrt{s_{NN}} < 8$ GeV in Au+Au collisions. A promising recent development is prediction of correlation between the directed flow and the angular momentum accumulated in the participant region of colliding nuclei [8, 15–19], which allows a deeper insight into collision dynamics.

The STAR-FXT (fixed-target) data on the directed flow of identified particles at energies $\sqrt{s_{NN}} = 3$ and 4.5 GeV were recently published in Refs. [20, 21]. These data were also analyzed within various, mostly kinetic models [11, 14, 22–33] in relation to various problems: the hyperon production [14, 26, 33], the production of light (hyper)nuclei [30, 31], etc. The EoS of the matter produced in the nucleus-nucleus collisions was the prime topic of the above theoretical considerations. It was discussed mostly in terms of softness and stiffness of the EoS [11, 22–24, 26, 29]. These studies were performed within different transport models: The relativistic version of the quantum molecular dynamics implemented into the transport code JAM [11], the hadronic transport code SMASH [22, 29], the Ultrarelativistic Quantum Molecular Dynamics (UrQMD) [23, 24], and a multiphase transport model [26].

All the aforementioned papers [11, 22–24, 26, 29] reported that stiff (to a different extent) EoS's are preferable for the reproduction of the directed flow (v_1) at $\sqrt{s_{NN}} = 3$ GeV, while the v_1 data at 4.5 GeV require a softer EoS. The latter was interpreted as indication of onset of the phase transition into QGP. This conclusion about preference of the stiff EoS at the energy of 3 GeV appears to contradict the earlier findings. The analysis of KaoS [34] and FOPI [35] data at collision energies $E_{lab} \leq 2A$ GeV ($\sqrt{s_{NN}} \leq 2.7$ GeV) within the Isospin Quantum Molecular Dynamics model led to the conclusion that the soft EoS with the incompressibility $K = 210$ MeV is strongly preferable [35–38]. Although, this energy range is somewhat below of the STAR-FXT one.

The energy range of the BNL Alternating Gradient Synchrontron (AGS), $E_{lab} = 2 - 10.7$ A·GeV ($\sqrt{s_{NN}} =$ 2.7-4.9 GeV), practically coincide with the currently explored STAR-FXT range. The results of the analysis of the AGS data [39, 40] are more controversial. Strong preference of the soft EoS was reported in Refs. [3, 4, 41–43]. In Refs. [3, 4], the EoS additionally softens at $\sqrt{s_{NN}} > 4$ GeV because of onset of the deconfinement transition. However, in Ref. [44] it was found that the best description of the data on the transverse flow is provided by a rather stiff EoS at 2A·GeV (NL3) while at higher bombarding energies (4–8 A·GeV) a medium EoS ($K = 300$ MeV) leads to better agreement with the data, while the differences in the soft-EoS and stiff-EoS transverse flows become of minor significance at 4–8 A·GeV. In Ref. [45], the proton flow was found to be also independent of stiffness of the EoS, however provided the momentum dependence in the nuclear mean fields is taken into account.

As recent studies [11, 22–26, 29, 32] of the STAR-FXT v_1 data deduced comparatively stiff EoS's at $\sqrt{s_{NN}} = 3$ GeV, some of them predicted comparatively low baryon densities (n_B) for onset of the denfinement transition.

*e-mail: yivanov@theor.jinr.ru
†e-mail: kozhevnikova@jinr.ru

PROCEEDINGS OF SCIENCE

Double Deeply Virtual Compton Scattering at Jefferson Lab Hall A

Marie Boër[a,*] **and Debaditya Biswas**[a]

[a] *Virginia Tech,*
Blacksburg, VA, USA.

E-mail: mboer@jlab.org

This paper presents our project and perspectives to measure for the first time beam spin asymmetries from Double Deeply Virtual Compton Scattering in the $eP \to e'P'\mu^+\mu^-$ reaction at Jefferson Lab. Our goal is to constrain the so-called Generalized Parton Distribution (GPDs) in a kinematic region that isn't accessible from other reactions, such as Deeply Virtual Compton Scattering, to allow for their extrapolation to "zero skewness", i.e. at a specific kinematic point enabling for tomographic interpretations of the nucleon's partonic structure. We are discussing DDVCS phenomenology and our approach, as well as our experimental project aimed at complementing the SoLID experiment at JLab Hall A with a new muon detector.

25th International Spin Physics Symposium (SPIN 2023)
24-29 September 2023
Durham, NC, USA

*Speaker

https://pos.sissa.it/

1. Introduction

The so-called Generalized Parton Distribution (GPDs) [1, 2] are matrix elements parametrizing the soft structure of the nucleon in "Hard Exclusive" reactions [3, 4]. GPDs contain information on the longitudinal momentum versus transverse position of the partons (quarks and gluons) [5, 6]. We have been studying GPDs for the last ~30 years as we are looking to move towards multidimensional images of the nucleon structure. One of the interesting interpretations of GPDs is the possibility to access tomographic views of the nucleon, where we can relate the transverse position of the partons to the quark and gluon densities [7]. This kind of interpretation relies on extrapolations of GPDs to certain kinematics that can't be accessed experimentally, and on models, referred to as "zero skewness" [8], i.e. reactions where all the momentum transferred to the nucleon is purely transverse. Our goal is to study Double Deeply Virtual Compton Scattering to constrain the GPDs at this limit.

"Hard Exclusive" reactions refers to: a "hard scale" of at least 1 GeV^2, allowing for factorization between a soft part parametrized by the GPDs, and a hard part, calculable [9]; "exclusivity" refers to all products of the reaction being known, enabling measurement of the total momentum transfer to the nucleon (we use Mandelstam variable "t", the squared momentum transfer). Fig.1 is the general Compton-like process, where a photon is scattered off a quark in the nucleon. We display the factorization lane, the bottom part representing the GPDs. The incoming and scattered photons have to be of different virtuality to allow for a non-zero momentum exchange to the nucleon. We can distinguish between 3 particular cases of "Compton Scattering": Deeply Virtual Compton Scattering (DVCS), where the incoming photon is virtual (spacelike) and the outgoing one is real; Timelike Compton Scattering (TCS), where the incoming photon is real and the outgoing one is virtual, subsequently decaying into a lepton pair; and Double Deeply Virtual Compton Scattering (DDVCS), where both photons are virtual. DVCS has been measured at multiple facilities [10–25], TCS has recently been measured for the first time at JLab [26], DDVCS has never been measured.

There are several GPDs, for quarks and gluons, and to account for relative helicity states of the quark-nucleon system. At leading order and leading twist (lowest order in photon's virtuality related to extra-gluon exchanges), for a spin 1/2 nucleon, we have 4 (x2 for quarks and gluons) chiral-even GPDs, and 4 (x2) chiral-odd GPDs (with quark helicity flip), i.e. 16 total (see for instance [5, 27]). These GPDs depend on 3 variables: t, x (nucleon's longitudinal momentum fraction carried by the parton), ξ ("skewness", related to the longitudinal momentum transfer to the quark in light cone frame). We will neglect here their evolution with the photons' virtuality (namely Q^2=-q^2 and/or Q'^2=q'^2 for incoming and outgoing photons, respectively, defined from their squared 4-momenta). GPDs can't be measured directly: we measure Compton Form Factors (CFFs), functions of the GPDs, accessible from fits of cross sections and asymmetries of the various reactions. Most models are currently constrained by measurements of DVCS only, where GPDs can only be accessed at specific kinematic points, for x=$\pm\xi$. TCS being the "time-reversal" equivalent of DVCS at leading order and leading twist [28], it accesses GPDs at the same kinematics. On the other hand, we can vary the relative virtualities of the two photons in DDVCS to access different kinematics, such as $|x| < \xi$ [5, 29, 30]. It is essential to deconvolute these 2 variables and extrapolate the GPDs to ξ=0 [8], which is needed for tomographic interpretations.

PROCEEDINGS OF SCIENCE

Future measurements of TCS at JLab Hall C

Debaditya Biswas[a,*] **and Marie Boër**[a]

[a] *Virginia Tech,*
Blacksburg, USA

E-mail: debadityab22@vt.edu, mboer@vt.edu

Generalized parton Distributions (GPDs) are important functions to understand the three dimensional structure of the nucleon. Deeply Virtual Compton Scattering is one of the reaction accessing GPDs, and has been measured for the past ~20 years. However, to move forward, we need to look for other reactions, such as Timelike Compton Scattering (TCS), its "time-reversal" equivalent. Indeed, accessing GPDs from both DVCS and TCS independently will allow us, for instance, to study their universality. Any assesment on GPD's universality would be a milestone in our field. In this article we discuss our preliminary studies on the feasibility of measuring unpolarized and beam polarized cross sections and beam spin asymmetry for TCS in the dilepton photoproduction reaction. For that purpose, we use a polarized photon beam and an unpolarized target at JLab Hall C. We will discuss our Geant4 simulations, with a dedicated detector setup along with the use of the SBS magnet for separating outgoing e^+, e^- pairs.

25th International Symposium on Spin Physics,
24-29 September 2023
Durham, NC, USA

*Speaker

https://pos.sissa.it/

1. Introduction

This article discuss our preliminary studies for measuring Timelike Compton Scattering (TCS, displayed Fig 1) at Jefferson Lab Hall C, off an unpolarized Liquid Hydrogen target and a circularly polarized high intensity photon beam. Measuring TCS cross sections and beam spin asymmetries with an unpolarized target, is very important to constrain the Generalized Parton Distribution (GPDs) [1, 2] . GPDs are sensitive to the longitudinal momentum versus transverse position structure of partons (quarks and gluons) in the nucleon [3]. They can't be accessed directly from experiments: we are actually measuring functions of GPDs, called Compton Form Factors (CFFs). There are several GPDs corresponding to different possible relative orientations of the helicity of particles involved in the reaction [4]. In our case, the observables we aim to measure are most sensitive to the GPD "H", the one which is insensitive to the quark and to the nucleon's helicities. GPD H is currently well constrained from DVCS measurements, and this is why we would like to obtain similar measurements from TCS, for a comparison, and for universality studies. Furthermore, GPDs are real functions, but CFFs that we are measuring are complex functions: from DVCS measurements, we better constrain the imaginary part of the CFFs. Our equivalent measurement with TCS is sensitive to both real and imaginary parts, and thus will bring more constraints on the real part of the amplitudes in a multi-channel CFF extraction approach. We refer to articles [5, 6] for the phenomenology of TCS off the proton and projections of observables.

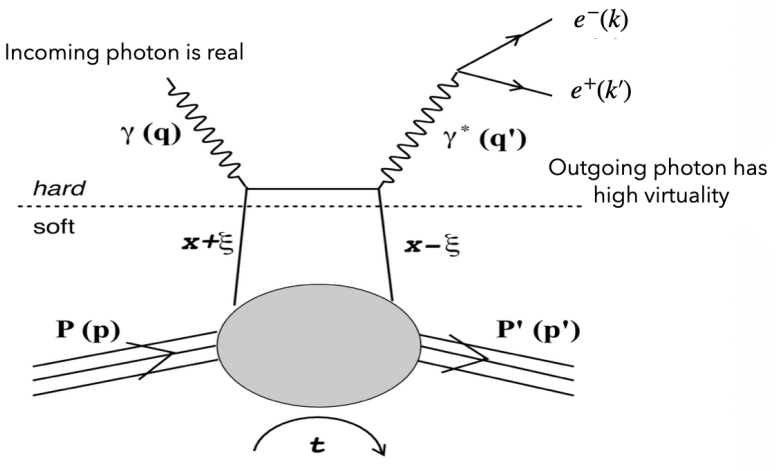

Figure 1: Time Like Compton Scattering (leading order and leading twist, CC not represented).

TCS is measured in the reaction $\gamma P \rightarrow e^+e^-P'$, where P is a nucleon (a proton here) and e is a lepton (an electron here). It interferes with another process, called Bethe-Heitler (BH) where the lepton pair is produced by a splitting of the incoming photon in the nucleon's field. BH is insensitive to the GPDs. It is parametrized by Form Factors. What we want to measure ("observables") is cross sections (σ) and beam spin asymmetries ($A_{\odot U}$ is mostly sensitive to the interference term in